https://doi.org/10.5194/acp-2021-121
Preprint. Discussion started: 12 March 2021

Atmospheric Chemistry and Physics Discussions

Unraveling Pathways of Elevated Ozone Induced by the 2020 Lockdown in Europe by an Observationally Constrained Regional Model: Non-Linear Joint Inversion of NO_x and VOC Emissions using TROPOMI

Amir H. Souri[1*], Kelly Chance[1], Juseon Bak[2], Caroline R. Nowlan[1], Gonzalo González Abad[1], Yeonjin Jung[1], David C. Wong[3], Jingqiu Mao[4,5], and Xiong Liu[1]

[1]Atomic and Molecular Physics (AMP) Division, Harvard–Smithsonian Center for Astrophysics, Cambridge, MA, USA

[2] Institute of Environmental Studies, Pusan National University, Busan, South Korea

[3]U.S. Environmental Protection Agency, Center for Environmental Measurement & Modeling, Research Triangle Park, NC, USA

[4]Geophysical Institute, University of Alaska Fairbanks, Fairbanks, AK, USA

[5]Department of Chemistry and Biochemistry, University of Alaska Fairbanks, Fairbanks, AK, USA

* Corresponding author: ahsouri@cfa.harvard.edu

Abstract. Questions about how emissions are changing during the COVID-19 lockdown periods cannot be answered by observations of atmospheric trace gas concentrations alone, in part due to simultaneous changes in atmospheric transport, emissions, dynamics, photochemistry, and chemical feedback. A chemical transport model simulation benefiting from a multi-species inversion framework using well-characterized observations should differentiate those influences enabling to closely examine changes in emissions. This approach has another advantage in that we can, to a certain extent, disentangle the chemical and physical processes involved in the formation of ozone. Accordingly, we jointly constrain NO_x and VOC emissions using well-characterized TROPOMI HCHO and NO_2 columns during the months of March, April, and May 2020 (lockdown) and 2019 (baseline). We observe a noticeable decline in the magnitude of NO_x emissions in March 2020 (14-31%) in several major cities including Paris, London, Madrid, and Milan expanding further to Rome, Brussels, Frankfurt, Warsaw, Belgrade, Kyiv, and Moscow (34-51%) in April. The large variability of changes in NO_x emissions is indicative of different dates and the degree of restrictions enacted to prevent the spread of the virus. For instance, NO_x emissions remain at somewhat similar values or even higher in northern Germany and Moscow in March 2020 compared to the baseline. Comparisons against surface monitoring stations indicate

https://doi.org/10.5194/acp-2021-121
Preprint. Discussion started: 12 March 2021


Atmospheric Chemistry and Physics Discussions

that the model estimate of the NO_2 reduction is underestimated, a picture that correlates with the TROPOMI frequency impacted by cloudiness. During the month of April, when ample TROPOMI samples are present, the surface NO_2 reductions occurring in polluted areas are described fairly well by the model (model: -21±17%, observation: -29±21%). Changes in VOC emissions are dominated by eastern European biomass burning activities and biogenic isoprene emissions. In March, however, TROPOMI HCHO sets an upper limit for HCHO changes such that the chemical feedback of NO_x on HCHO constrained by TROPOMI NO_2 reveals a non-negligible decline in anthropogenic VOC emissions in Paris (-9%), Milan (-29%), London (-5%), and Rome (-5%). Results support an increase in surface ozone during the lockdown. In April, the constrained model features a reasonable agreement with maximum daily 8 h average (MDA8) ozone changes observed at the surface (r=0.43), specifically over central Europe where ozone enhancements prevail (model: +3.73±3.94%, +1.79 ppbv, observation: +7.35±11.27%, +3.76 ppbv). Results of integrated process rates of MDA8 surface ozone over central Europe in the same month suggest that physical processes (dry deposition, advection and diffusion) decrease ozone on average by -4.83 ppbv, while ozone production rates dampened by largely negative $J_{NO2}[NO_2]$-$k_{NO+O3}[NO][O_3]$ become less negative, leading ozone to increase by +5.89 ppbv. Experiments involving fixed anthropogenic emissions suggest that meteorology (mainly as air temperature and photolysis) contributes to 42% enhancement in MDA8 surface ozone over the same region with the remaining part (58%) coming from changes in anthropogenic emissions. Results illustrate the capability of satellite data of major ozone precursors to help atmospheric models capture the essential character of ozone changes induced by abrupt emission anomalies.

1. Introduction

Continuous monitoring of air pollution by satellites can help our understanding of both anthropogenic and biogenic variability and change caused by rapid economic recession [Castellanos and Boersma, 2012] and regulations [Krotkov et al., 2016; Souri et al., 2020a]. Earth's atmosphere has exponentially become more polluted during previous decades because of rapid industrialization increasing anthropogenic emissions [Li and Lin, 2015], thus any abrupt hiatus in these emissions should result in an impulsive and sweeping impact on relatively short lifetime pollutants such as nitrogen dioxide (NO_2), formaldehyde (HCHO), and tropospheric ozone (O_3). The beginning of the global COVID-19 pandemic in early 2020 [Fauci et al., 2020] provided such an abrupt change in human activities [Le Quéré et al., 2020]. A first step to fully understand how

https://doi.org/10.5194/acp-2021-121
Preprint. Discussion started: 12 March 2021


Atmospheric Chemistry and Physics Discussions

much of these impacts are related to the pandemic lockdowns is to disentangle the physical and chemical processes determining their ambient concentrations. Unraveling those processes require precise, continuous observations of physical and chemical states and emission rates, which are not routinely available on global, continental and regional scales. Therefore, we resort to using a model realization attempting to reproduce such an intricate system. Models without observational guidance are incapable of numerically representing the real world [Lorenz, 1963], so our best option to improve a model is to constrain some of its prognostic inputs using well-characterized observations. Accordingly, the framework of this study is centered around inverse modeling and data assimilation.

Significant attention has been given to documenting the lockdown-related changes in atmospheric compositions around the world using both in-situ and satellite observations [e.g., Sicard et al., 2020; Shi and Brasseur, 2020; Lee et al., 2020; Salma et al., 2020; Le Quéré et al., 2020; He et al., 2020; Le et al., 2020; Miyazaki et al., 2020; Liu et al., 2020; Barré et al., 2020; Goldberg et al., 2020; Ordóñez et al., 2020; Wyche et al., 2021]. The broad picture is consistent among these studies; the lockdown drastically reduced the concentrations of NO_x, CO, and SO_2 and some types of particulate matters, whereas the concentrations of several secondarily formed compounds such as ozone increased due to emissions and/or meteorology. To the best of our knowledge, changes in volatile organic compounds (VOCs) due to the lockdown over Europe have not been reported.

The motivations of this study are to determine the capability of a regional model constrained by satellite HCHO and NO_2 columns to capture near-surface pollution, and if local ozone production rates are the driving factors for heightening ozone pollution during the 2020 lockdown. In other words, what chemical and physical processes are associated with the elevated ozone? How representative are satellite observations at capturing surface air quality through an inversion context? Is meteorology the primary factor in shaping elevated ozone as suggested by Ordóñez et al. [2020]?

To address these pivotal questions, it is desirable to constrain models using multi-species observations because relationships between the atmospheric compounds such as HCHO and NO_2 are importantly intertwined [Marais et al., 2012; Valin et al., 2016; Wolfe et al., 2016; Souri et al., 2020a,b]. Accordingly we build our inversion framework upon a non-linear joint analytical inversion of NO_x and VOCs proposed in Souri et al. [2020a] using TROPOMI HCHO and NO_2

https://doi.org/10.5194/acp-2021-121
Preprint. Discussion started: 12 March 2021


Atmospheric Chemistry and Physics Discussions

observations in Europe. Performing this type of inversion not only enables us to precisely quantify the impact of the pandemic on emissions (along with its uncertainty, as the inversion framework is analytical) but also paves the way for estimating the resulting changes on different pathways of surface ozone.

2. Measurements, Modeling, and Methods

2.1. Satellite Observations

2.1.1. TROPOMI NO_2

We use daily offline S5P TROPOMI tropospheric NO_2 slant columns [Copernicus Sentinel data processed by ESA and Koninklijk Nederlands Meteorologisch Instituut (KNMI), 2019] derived from a two-step framework involving DOAS spectral fitting in conjunction with a stratosphere/troposphere decoupler [Boersma et al., 2018]. The time periods of this study are March, April and May 2020 and 2019. The data provide Jacobians of light intensity with respect to optical thickness (i.e., vertically-resolved scattering weights) which are dependent on scene surface reflectivity, the cloudiness of the assumed Lambertian clouds, and sensor viewing geometry. Aerosol effects on the scattering weights are not taken into consideration. The 2019 TROPOMI observations used in this study have a spatial resolution of 7×3.5 km^2, whereas those in 2020 have a spatial resolution of 5.5×3.5 km^2. The NO_2 products for the study time period were produced by processor versions v01.02.02 (1 March 2019 – 20 March 2019) and v01.03.02 (20 March 2019 onward). The v01.03.02 processor includes an update to the FRESCO-S cloud algorithm and improvements to a quality flag variable. NO_2 validation from processors v01.02.02 and v01.03.02 shows similar biases and dispersion [Lambert et al., 2020], as do comparisons from before and after the pixel spatial resolution change [Verhoelst et al., 2021]. We extract good quality pixels based on the main quality flag (qa_flag) > 0.75, which removes retrievals flagged as bad and pixels over snow/ice or with cloud radiance fractions > 0.5, and resample them to our 15-km regional model (discussed later) using bilinear interpolation. Since vertical column densities (VCDs) depend on assumed gas profile shape (i.e., they are quasi-observations), we recalculate those shape factors using profiles from our constrained chemical transport model.

https://doi.org/10.5194/acp-2021-121
Preprint. Discussion started: 12 March 2021


Atmospheric Chemistry and Physics Discussions

Satellite remote sensing observations are usually far more stable than they are accurate. This can make the data practical for measuring relative changes in emissions, but may necessitate the use of a bias correction for absolute emissions estimates. Moreover, the systematic and random errors associated with satellite retrievals may differ markedly from location to location. It is therefore crucial to thoroughly validate columns against independent observations. To this end, we compile statistics reported in several validation studies focusing on the TROPOMI tropospheric NO_2 product and summarize their findings in Table 1. The most comprehensive global study to date is a comparison of TROPOMI tropospheric NO_2 with that derived from 19 MAX-DOAS instruments [Verhoelst et al., 2021]. This study indicates there is a low bias in TROPOMI tropospheric NO_2 of -23 to -37% relative to MAX-DOAS at clean to moderately polluted sites, and as large as -51% at highly polluted sites. When considering all sites, the overall median bias in this study was found to be -37%, with a RMSE of 3.5×10^{15} molec/cm^2 (defined as half of the 68% interpercentile). No obvious seasonal patterns were found in the biases. These results are consistent with other validation studies which have observed a low bias in TROPOMI tropospheric NO_2 [Chan et al., 2020; Griffin et al., 2019; Judd et al., 2020]. A potential significant source of bias in polluted regions is the relatively low-spatial resolution (1×1^o) TM5-MP prior profiles used in the TROPOMI air mass factor calculation. Several validation studies have shown the low bias in TROPOMI NO_2 can be reduced in polluted regions by 5-17% through the use of higher spatial resolution model a priori profiles or other improvements in the AMF calculation [Chan et al., 2020; Griffin et al., 2019; Judd et al., 2020; Zhao et al., 2020]. There are challenges in using the aforementioned numbers, of which the largest relates to the lack of formulating errors as functions of prognostic inputs used for the retrievals (e.g., albedo, scene radiance, etc.). This in turn precludes a more general estimation of errors for all pixels. Given the fact that our study will derive emissions primarily from information in moderate to highly polluted areas [Souri et al., 2020a], we uniformly scale up NO_2 pixels by 25% based on the low bias determined by Verhoelst et al. [2021] while considering the potential reduction in the bias through the use of higher spatial resolution trace

https://doi.org/10.5194/acp-2021-121
Preprint. Discussion started: 12 March 2021


Atmospheric Chemistry and Physics Discussions

gas a priori profiles. We set the RMSE to 1.1×10^{15} molec/cm^2 ($<6\times10^{15}$ molec/cm^2) in clear regions and 3.5×10^{15} molec/cm^2 ($>=6\times10^{15}$ molec/cm^2) in moderately to highly polluted regions.

2.1.2. TROPOMI HCHO

We use daily offline S5P TROPOMI HCHO total slant columns [Copernicus Sentinel data processed by ESA, German Aerospace Center (DLR), 2019]. A full description of the algorithm can be found in De Smedt et al. [2018]. The HCHO products for the study time period were produced by processor versions v01.01.05 (1 March 2019 – 28 March 2019), v01.01.06 (28 March 2019 – 23 April 2019) and v01.01.07 (23 April 2019 onward). The newer versions have added updates to the surface classification climatology and cloud products that might have some effects on the magnitude of HCHO in cloudy scenes. We again remove bad pixels based on qa_flag < 0.75 and recalculate shape factors using the simulated profiles derived from our regional model.

Validation efforts reported in the sixth Quarterly Validation Report of the Copernicus Sentinel-5 Precursor Operational Data Products [Lambert et al., 2020] indicate varying biases depending on the magnitude of HCHO concentrations in comparison to ground-based observations. Locations with HCHO concentrations above 8×10^{15} molec/cm^2 show a low bias of ~-31%. Conversely, clean sites with HCHO concentrations below 2.5×10^{15} molec/cm^2 undergo a high bias of 26%. Those biases oscillate around 8×10^{15} molec/cm^2. Vigouroux et al. [2020] expanded the validation suite by including more than 25 FTIR stations majorly located over pristine areas and 9 MAX-DOAS stations located in polluted sites. Results from the comparison with FTIR measurements (over clean areas) indicate a high bias, whereas those compared with MAX-DOAS measurements at Cabauw and De Bilt (Netherlands) show a low bias of -44%. The agreement between MAX-DOAS and satellite observations improved after adjusting TROPOMI shape factors based on MAX-DOAS observations. By compiling numbers quoted in Lambert et al. [2020] and Vigouroux et al. [2020], we correct the existing biases in TROPOMI HCHO by scaling 25% ($<2.5\times10^{15}$ molec/cm^2) down columns in clear areas and 30%

https://doi.org/10.5194/acp-2021-121
Preprint. Discussion started: 12 March 2021


Atmospheric Chemistry and Physics Discussions

(>=7.5×10^{15} molec/cm^2) up in polluted areas. We set the magnitude-dependent RMSE to be equal to 4% of HCHO total columns based on Vigouroux et al. [2020].

2.1.3. MODIS AOD

To improve the simulation of total aerosol mass, we use the collection 6 MODIS aerosol optical depth (AOD) from both Aqua (~ 13:30 LT) and Terra (~ 10:30 LT) platforms over both land and ocean [Levy et al., 2013] (available at https://ladsweb.modaps.eosdis.nasa.gov, access May 2020). We independently validate all three major products, namely the deep blue, the dark target and a combined dark blue products by comparing to AOD values measured by AERONET over Europe at the same time period of this study. Only good and very good (qa>=2) pixels are selected for the comparison. The AERONET AOD data are computed based on the values at 500 nm and Angstrom Exponent in the 440-675 nm range. We collocate two datasets if they are within 10 km radius and less than 30 mins apart. The dark blue product results in the best agreement (r>0.87) with a high bias of <0.05 (Figure S1, and S2). We remove the bias and assign the value of the covariance matrix of observations to the RMSE values obtained from the comparison.

2.2. Surface Measurements

UV photometry and chemiluminescence surface ozone and NO_2 measurements all over continental Europe are used to investigate possible changes in their concentrations induced by the lockdown (https://discomap.eea.europa.eu/map/fme/AirQualityExport.htm, access June 2020). The NO_2 chemiluminescence measurements are usually overestimated due to interferences from the NO_z family (PAN, organic nitrate, HNO_3, etc.). We assume that the interferences are not significantly different between the baseline and lockdown mainly due to relatively low photochemistry in early spring [Lamsal et al., 2008] compared to summertime.

More than 6450 meteorological stations archived on NOAA's integrated surface database (https://www.ncei.noaa.gov/data/global-hourly/, access April 2020) are used to validate the performance of our weather model in terms of several prognostic inputs including ambient air temperature, air humidity, and U and V wind components.

https://doi.org/10.5194/acp-2021-121
Preprint. Discussion started: 12 March 2021


Atmospheric Chemistry and Physics Discussions

2.3. WRF-CMAQ Modeling

The regional air quality simulations at 15×15 km^2 are carried out with the widely used CMAQ v5.2.1 (https://doi.org/10.5281/zenodo.1212601) in conjunction with WRF v3.9.1 [Skamarock et al. 2008] models. The models overlap and cover continental Europe and some portions of Africa and Middle East. The domain consists of 483 east-west, 383 north-south grids, and 37 unevenly spaced eta levels (Figure 1). The simulation time period is from March to May 2019 and 2020 (six months). Since IC/BC are taken from already spun-up National Centers for Environmental Prediction (NCEP) FNL (final) reanalysis and GEOS-Chem v12.9.3 (10.5281/zenodo.3974569) runs, we only spin up the models for the month of February. The chemistry configuration of the CMAQ model mainly consists of CB05 with chlorine chemistry (gases) and AERO6 (aerosol). Biogenic emissions are processed by the offline standalone Model of Emissions of Gases and Aerosols from Nature (MEGAN) v2.1 model [Guenther et al., 2012] based on high-resolution plant functional maps made by Ke et al. [2012]. Anthropogenic emissions are based on the Community Emissions Data System (CEDS) inventory in 2014 [Hoesly et al., 2018]. We also output the CMAQ integrated process analysis quantifying the contribution of each process to the amount of compounds. The physical setting of WRF includes the Lin microphysics scheme [Lin et al., 1983], the Grell 3-D ensemble cumulus scheme [Grell and Dévényi, 2002], the RRTMG radiation scheme, ACM2 planetary boundary layer parametrization [Pleim, 2007], and Pleim-Xu land-surface scheme [Xiu and Pleim, 2001]. We nudge moisture, wind and temperature fields toward the reanalysis data used only outside of the PBL layer. Moreover, leaf area index and the sea surface temperature are updated every 6 hours based on satellite measurements included in the reanalysis data. Extensive model evaluations based upon surface observations show a striking correspondence (Table S1, S2) which is indicative of fair energy budget and transport in our model.

2.4. Inverse Modeling and Data Assimilation

To adjust the bottom-up emission inventories, we follow a non-linear joint inversion method proposed in Souri et al. [2020a]. Briefly, a Gauss-Newton algorithm is utilized to incrementally solve the Bayes' quadratic function in analytical fashion. The posterior emissions are then derived by

$$\mathbf{x}_{i+1} = \mathbf{x}_a + \mathbf{G}[\mathbf{y} - F(\mathbf{x}_i) + K_i(\mathbf{x}_i - \mathbf{x}_a)] \quad (1)$$

https://doi.org/10.5194/acp-2021-121
Preprint. Discussion started: 12 March 2021


Atmospheric Chemistry and Physics Discussions

where $\boldsymbol{y}$ is bias-corrected TROPOMI NO_2 and HCHO observations, $\mathbf{x}_a$ (or $\mathbf{x}_0$) is the prior emissions, $\mathbf{x}_i$ is the posterior emission at the *i*th increment, F is the forward model (here WRF-CMAQ) to project the emissions onto columns space, **G** is the Kalman gain,

$$\mathbf{G} = \mathbf{S}_e \, K_i^T \left(K_i \mathbf{S}_e \, K_i^T + \mathbf{S}_o \right)^{-1} \quad (2)$$

and K_i $(= K(\mathbf{x}_i))$ is the Jacobian matrix calculated explicitly from the model using the finite difference method. $\mathbf{S_o}$ and $\mathbf{S_e}$ are the error covariance matrices of the observations and emissions. In terms of the prior errors, we use the numbers reported in Souri et al. [2020a]. The instrument covariance matrices are populated with squared-sum of the aforementioned RMSEs based on the compilation of the validation studies and precision errors provided with the data. Both error matrices are diagonal. The inversion window is monthly. The covariance matrix of the a posteriori is calculated by:

$$\hat{\mathbf{S}}_e = (\mathbf{I} - \mathbf{G}\hat{K} \;)\mathbf{S}_e \quad (3)$$

where $\hat{K}$ is the Jacobian from the i*th* iteration. Here we iterate Eq.1 three times. The averaging kernels (**A**) are given by:

$$\mathbf{A} = \mathbf{I} - \hat{\mathbf{S}}_e \mathbf{S}_e^{-1} \quad (4)$$

Not only does this method considers non-linear chemical feedback among NO_2-HCHO-NO_x-VOC by simultaneously incorporating the HCHO and NO_2 in the inversion framework, it also permits quantification of **A** that explicitly explains the amount of information obtained from the observation.

We also correct total aerosol mass by daily assimilating the MODIS dark blue AOD observations following the algorithm discussed in Jung et al. [2019]. Briefly, the assimilation framework uses a modified optimal interpolation method adjusting uniformly all relevant aerosol masses in a column as a function of a weighted-distance and appropriate errors.

3. Results and Discussion

3.1. Variability of HCHO and NO_2 columns seen by TROPOMI

We assess difference maps of TROPOMI HCHO and NO_2 columns in 2020 with respect to those in 2019 during the months of March, April and May. The difference maps along with the absolute values of the tropospheric NO_2 columns are shown in Figure 2. Regardless of the year, we observe a noticeable reduction in NO_2 as we approach warmer months which can be explained

https://doi.org/10.5194/acp-2021-121
Preprint. Discussion started: 12 March 2021


Atmospheric Chemistry and Physics Discussions

by increases in OH concentrations (higher water vapor content, solar radiation, and O_3 levels), faster vertical mixing due to larger sensible fluxes (more diluted columns due to stronger advection in higher altitudes), and a reduction in temperature-dependent light-duty diesel NO_x emissions [Grange et al., 2019]. Two unintended consequences of this sequential decline, noted by Silvern et al. [2019] and Souri et al. [2020a], are first the free-tropospheric region complications and second a barrier to obtaining high amount of information from the sensor which manifests itself in lower averaging kernels of emission estimates (shown later). The anomaly map in March indicates pronounced decreases in tropospheric NO_2 columns over several countries including France, Spain, Italy, and Germany (box A). In contrast, we see negligible reductions in the magnitude of the NO_2 columns over some portions of the UK excluding London (box B), northern Germany (box C), and Moscow, Russia (box D). A very recent study [Barré et al. 2020] observed roughly the same tendency which was attributable to meteorological changes. While those changes are indeed an important piece of information that will be investigated later in this study, we should recognize that the degree of the enforced restrictions varies both spatially and temporally; moreover changes in emission heavily rely on the dominant emission sector (e.g., mobile or industry) and population. For instance, northern Germany is associated with less populated areas and industrial areas which might be less impacted by the shutdown (see Figure 2 in Le Quéré et al. [2020]), and as a result, we would expect a weaker signal in the reduction of NO_2. According to TASS press [https://tass.com/society/1144123, accessed Sep 2020], Russian governments did not take significant measures to control the virus before April 15, immediately evident in the large NO_2 enhancement over Moscow in March (box D). During the next two months (April and May), we observe a major turnaround over this city (box F and H). In May, the anomaly of the tropospheric NO_2 suggests an abrupt hiatus in the ongoing reduced NO_x emissions in central Europe (box G). However it is crucial to note that these maps are based upon sporadic clear-sky pixels that might obscure the full portrayal of emissions changes happening throughout the period (discussed later).

We further investigate potential changes in HCHO total columns shown in Figure 3 in the same context as we discussed for NO_2. Various VOCs with different sources contribute to the formation of HCHO (see Figure 2 in Chan Miller et al. [2016]) leading to striking HCHO column patterns with large variations. In theory, we have a higher chance to single out anthropogenic-derived HCHO concentration by looking at wintertime measurements, although temperature and

https://doi.org/10.5194/acp-2021-121
Preprint. Discussion started: 12 March 2021


Atmospheric Chemistry and Physics Discussions

photochemistry are always key influencers of oxidizing/photolyzing all types of VOCs. The inevitable trade-off for this is dealing with a weaker signal that is near to instrument detection limit. Encouragingly, the TROPOMI HCHO retrieval offers a very low detection limit for individual pixels (7×10^{15} molec/cm^2) that can be further lowered down by co-adding measurements (roughly a factor of $1/\sqrt{n}$). Accordingly, we observe a promising signal in March over eastern European countries that is not explainable by biogenic emissions; but the magnitudes of the difference over these areas ($<1.5\times10^{15}$ molec/cm^2) are below the detection limit ($\sim 2.4\times10^{15}$ molec/cm^2 given the co-added measurements over time) to relate them to the lockdown in a robust manner; nonetheless TROPOMI sets an upper limit for these changes. In April, results show elevated HCHO concentrations in high latitudes in 2019 (box I), mainly a result of biomass burning activities in eastern Europe [e.g., Karlsson et al. 2013]. As temperature rises in May, the footprint of biogenic emissions become more visible. This signal is not only induced by the inherent temperature-dependency of biogenic isoprene emissions, but also stems from the fact that isoprene reactivity significantly increases by rising temperature [Pusede et al. 2015]. The dipole anomaly of HCHO columns suggested by TROPOMI (box J and K) pertains largely to variations in ambient surface air temperature (shown later).

3.2. Top-Down estimates of NO_x and VOC emissions

Following the inversion and the data assimilation frameworks, we adjust the total amounts of VOC, NO_x emissions, and aerosols mass using the well-characterized TROPOMI HCHO, NO_2 and MODIS AOD observations for the study time period. We focus on the topic of gas phase chemistry (i.e., ozone and its precursors) implying that the aerosol data assimilation is carried out to partially remove errors associated with radiation [e.g., Jung et al., 2019] or heterogenous chemistry [Jacob, 2000], therefore, the aspect of aerosol changes induced by the lockdown will be examined elsewhere. The spatial distributions of magnitude of the top-down NO_x and VOC emissions (i.e., constrained by the observations), their corresponding changes and averaging kernels are shown in Figure 4 and Figure 5, respectively. It is worth emphasizing that we use identical prior values in terms of anthropogenic emissions in both years; therefore, the differences in the top-down emissions are primarily dictated by the observations used in the inversion. According to Figure 4, large averaging kernels associated with NO_x emissions are confined in high-emitting regions suggesting that the most valid estimates can be found in areas undergoing strong TROPOMI NO_2 signals. We observe a large reduction (31-45%) in the bias associated with

https://doi.org/10.5194/acp-2021-121
Preprint. Discussion started: 12 March 2021


Atmospheric Chemistry and Physics Discussions

simulated surface NO_2 using the posterior emissions compared to the surface measurements in Europe, although improvements in correlation were minimal (not shown). Similarly, as expected, the discrepancies between the simulated tropospheric NO_2 columns versus TROPOMI are largely mitigated by the inversion (Figure S3 and S4). Immediately apparent in Figure 4 is a strong correlation between anomaly maps of TROPOMI tropospheric NO_2 (Figure 2) and those of top-down emissions. However, in practical terms, the magnitude of these anomalies is not as drastic as the ratio of observation to model ratio because of the consideration of observational errors and chemical feedback [Souri et al., 2020a], which always leaves some doubt about the practicality of direct mass balance methods. We observe reductions in NO_x emissions in March (14-31%) in several major cities including Paris, London, Madrid, and Milan; the reductions further expand to Rome, Brussels, Frankfurt, Warsaw, Kyiv, Moscow, and Belgrade with higher magnitudes (34-51%) in April. Table 2 summarizes the absolute and relative differences in total NO_x emissions estimated by the inversion binned to different regions in Europe based on country land borders. In general, the level of NO_x reduction is somewhat higher in April relative to months of March and May owing to spatiotemporal variabilities associated with the restrictions; for example, UK and Poland governments enforced the restrictions starting in the last week of March to the middle of April, a situation that clearly shows up in our results. Interestingly, the decreased anthropogenic NO_x emissions in the strait of Gibraltar and Alboran Sea reveal reportedly reduced ship activities [United Nations Conference on Trade and Development Report, Accessed Dec 2020]. The numbers in May indicate that several countries in central and eastern Europe (shown in box G in Figure 2) likely eased coronavirus lockdown restrictions, a picture that has yet to be verified by surface measurements (discussed later).

As to VOC emissions, we observe a significant improvement in the magnitude and spatial distribution of simulated HCHO columns after the inversion with respect to TROPOMI data (Figure S5 and S6). It is very evident that the magnitudes of the emissions primarily follow anthropogenic sources in March; expectedly, very low averaging kernels over major European cities in this month are indicative of inadequacies of one-month averaged TROPOMI HCHO data. However, we surprisingly observe a noticeable decline in the amount of VOC emissions (majorly anthropogenic) in Paris (-9%), Milan (-29%), London (-5%), and Rome (-5%). All of these cities emit considerable amounts of VOCs during wintertime [Schneidemesser et al., 2011; Possanzini et al., 2002; Baudic et al., 2016]. This tendency, which is striking, mainly stems from the indirect

https://doi.org/10.5194/acp-2021-121
Preprint. Discussion started: 12 March 2021


Atmospheric Chemistry and Physics Discussions

impacts of the reduced NO_x emissions on HCHO formation [Marais et al., 2012; Valin et al., 2016; Wolfe et al., 2016; Souri et al., 2020b]. The sensitivity of HCHO levels to VOC emissions is controlled by the availability of OH that is impacted by NO_x. A decrease in NO_x emissions in NO_x-saturated areas frees up more OH to faster oxide VOCs [Souri et al., 2020b] resulting in a steeper gradient of HCHO with respect to its sources. Likewise we observe larger Jacobians of HCHO with respect to VOC emissions in 2020 over the cities mentioned (not shown). If we assume the relative changes in HCHO levels between the two years to be insignificant, which are suggested by TROPOMI HCHO (considering the errors in the retrieval), the steeper gradient of HCHO concentrations with respect to VOC emissions should normally lead to a reduction in the VOC emissions in 2020. In other words, it would require a smaller VOC emission rate to reach to the same amount of HCHO. We note that the TROPOMI HCHO observations provide an upper limit of the changes so that we can make this assumption. Table 3 summarizes the amount of VOCs changing in the cities mentioned. The inversion partly corrects for the large underrepresentation of biomass burning emissions in high latitudes occurring in April 2019 but due to large uncertainties of the retrieval over this area, averaging kernels are low. We revisit the pronounced dipole anomaly of dominantly biogenic VOC emissions in May. It is readily evident from the averaging kernels that more realistic information from TROPOMI HCHO is attainable in warmer months, contrary to the NO_2 case.

3.3. Disparities and rationale behind the differences in near-surface concentrations suggested by the constrained model versus those by in-situ measurements

3.3.1. NO_2 and HCHO

We further investigate the effect of the lockdown on the surface HCHO and NO_2 concentrations based on the constrained simulations. Figure 6 gives the difference maps (lockdown minus baseline) of daily-averaged surface NO_2 and HCHO overplotted with the differences of surface wind vectors, planetary boundary layer heights (PBLHs), surface air temperature, and the ratio of photolysis rates below clouds (J_{below}) to those in clear-sky conditions (J_{clear}) following Madronich [1987]. The anomaly of emissions is on par with those of surface NO_2 and HCHO surface concentrations, this is perhaps not surprising, since the emissions are mostly located near the surface. Horizontal transport (shown as wind vectors) plays a critical role in explaining the spatial variations in emissions downwind.

https://doi.org/10.5194/acp-2021-121
Preprint. Discussion started: 12 March 2021


Atmospheric Chemistry and Physics Discussions

PBLH describes the level of vertical diffusion of air parcels [Jacobson, 2005]. The increase (decrease) in the PBLH is an indication of more (less) diluted air, subject to assuming that the pollutant concentration (in mixing ratio) would exponentially decrease aloft. The extent to which PBLH can impact air pollution relative to advection is strongly dependent upon the wind speed (see Figure 8 in Su et al., [2018]). The stronger the wind, the more likely PBLHs are going to be of secondary importance. We subjectively identify calm conditions by assuming that wind speeds should be below 1 m/s. We overlay the calm conditions as black dots over the PBLH contour. Although model uncertainties exist, the less pronounced NO_2 reduction over UK and northern Germany in March is unlikely to be resulting from shallower PBLHs in 2020 given how strong the predominant winds are. A strong expansion of PBL over the central Europe in April and May 2020 relative to 2019 possibly contributes to a larger reduction of NO_2 concentration.

Because of relatively colder air and less photochemistry in March, VOCs become naturally less reactive. This in turn will provide an opportunity for the volume of air to become dispersed. Thus the reduced VOC emissions over several major cities influence larger areas and become less distinctive. The temperature dependency of HCHO concentration progressively becomes more pronounced with increasing temperature. Both photochemistry and biogenic derived emissions are a function of shortwave solar radiation [Madronich, 1987; Guenther et al., 2012; Stavrakou et al., 2014] that can vary significantly with cloud transmissivity and the solar zenith angle. The ratio of J_{below}/J_{clear} well describes such a relationship; positive (negative) differences in the ratio suggest more (less) photochemistry. The strongly positive ratio of J_{below}/J_{clear} over the central Europe in April potentially overrides the fluctuations associated with surface temperature leading HCHO levels to rise.

Clearly, with the help of the CMAQ process analysis, more quantitative work on relevant physical/chemical processes pertaining to NO_2 and HCHO surface concentrations can be done here, but before proceeding it is necessary to examine whether the constrained model can adequately represent the changes observed by surface measurements. Unfortunately we limit the analysis to NO_2 due to the lack of routinely measured HCHO observations. Several factors can complicate this analysis: i) having overconfidence in the constrained model where the satellite observations used were uncertain; this problem can be safely addressed by considering grid cells whose averaging kernels are above a threshold (here 0.5), ii) ignoring spatial representivity function to directly compare point measurements to the model grids; a statistical construction of

https://doi.org/10.5194/acp-2021-121
Preprint. Discussion started: 12 March 2021


Atmospheric Chemistry and Physics Discussions

the spatial representivity function [Janic et al., 2016] requires a dense observational network so that we can build a semivariogram; instead, we only consider model grid cells having more than two stations; those observations then are then averaged, iii) interferences of NO_z family on NO_2 chemiluminescence measurements [Dickerson et al., 2019] which can be partly discounted when calculating differences, iv) model uncertainties, especially with respect to turbulent and convective fluxes that are heavily determined by representing local heterogenicity of forces and non-hydrostatic dynamics [Emanuel, 1994], all of which are challenging to properly resolve in a 15-km resolution. With these caveats in mind, we plot the daily-averaged changes of surface NO_2 concentrations in 2020 relative to 2019 derived by the model and the European air quality network for the months of March, April, and May (Figure 7). Large gaps in Figure 7 are caused by considering grid cells with averaging kernels>0.5 and number of samples>2. The constrained model correlates reasonably well with the changes observed by the surface measurements in March and April, but it fails to reflect those in May. The surface measurements reinforce the less pronounced reduction in NO_2 in northern Germany and UK, although the magnitudes are not as large as those suggested by the model. The constrained model tends to consistently underrepresent the decline in NO_2 in March (model: -11±21%, observation: -19±16%), April (model: -21±17%, observation: -29±21%), and May (model: -12±18%, observation: -25±20%). The frequency of TROPOMI data heavily impacted by cloudiness is another factor that can effectively lead to the underrepresentation of the model in a course of a month. Figure 8 depicts the number of days that TROPOMI was able to sample on. There is a strong degree of correlation between the frequency of the data and the discrepancy between the model versus the surface observations. This is especially the case for May when we see too few days to be able to realistically reproduce NO_2 changes. Given the reasonable performance of our model at reproducing the changes observed over the surface in April, a result of abundant samples from TROPOMI, we only focus on this month for the subsequent analysis.

3.3.2. Ozone

Figure 9 depicts the changes in maximum daily 8 h average (MDA8) surface ozone concentrations suggested by the measurements and the constrained model in April. Immediately obvious from the observations is the elevated surface ozone concentrations up to 32% in places where NO_x emissions drastically decreased such as Germany, Italy, France, UK, Switzerland, and Belgium (shown as box L). This tendency potentially is driven by ozone chemistry [Sicard et al.,

https://doi.org/10.5194/acp-2021-121
Preprint. Discussion started: 12 March 2021


Atmospheric Chemistry and Physics Discussions

2020a; Shi and Brasseur, 2020; Grange et al. 2020; Salma et al., 2020; Lee et al., 2020] and/or meteorology [Lee et al., 2020; Wyche et al., 2021; Ordóñez et al., 2020] has drawn much attention. The challenge is to simulate a model that is the characteristic of such a complex tendency [e.g., Parrish et al., 2014]. Encouragingly, our constrained model does have skill in describing the essential character of the ozone enhancements over the whole domain (r=0.43). In the proximity of central Europe (shown as box L), the enhanced MDA8 ozone concentration observed by the observations is 7.35±11.27% (+3.76 ppbv) which is nearly a factor of two larger than that of the model (3.73±3.94%, +1.79 ppbv).

While the remaining model uncertainty could be either improved or characterized by including more observations (if available), reconfiguring the physical/chemical mechanisms used, and constraining chemical boundary conditions, it is imperative to gauge the contribution of each process (i.e., transport, chemistry, etc.) in forming ozone changes. Here we mainly make use of the CMAQ process analysis. A direct use of the process analysis output (in unit of ppbv hr^{-1}) can be confusing as both physical/chemical processes and underlying concentrations are inextricably linked together. To be able to isolate each process (in unit of hr^{-1}), we normalize the outputs by ozone concentrations. Here, we average each process at the same hours used in calculating MDA8. Figure 10 shows the major model processes, namely as horizontal transport (horizontal advection plus diffusion), vertical transport (vertical advection plus diffusion), dry deposition, and chemistry in 2020, 2019, and their differences. Positive (negative) values indicate a source (sink) for ozone. Regarding the horizontal transport, the values mostly follow the transport pattern and are dependent on whether the advected air mass is more or less polluted. The vertical transport correlates with the PBLH which is an indicator of the atmospheric stability and turbulence, although we should not rule out the impact of the subgrid convective transport that can occur sporadically. Low PBLHs are usually associated with more stable (or sometimes capping inversion) and weaker vertical mixing [e.g., Nevius and Evans, 2018]. Vertical transport which is majorly dictated by the vertical diffusion is by far the most influential factor in the magnitude of ozone [e.g., Cuchiara et al., 2014]. In contrast to NO_2 and HCHO, a stronger vertical diffusion increases surface ozone due to positive gradients of ozone with respect to altitude. However, the aerodynamic resistance controlling dry deposition velocity [Seinfield and Pandis, 2006] is also a function of turbulent transport. For example, during daytime, intensified turbulence exposes more pollution to surface deposition. It is because of this reason that we see the dry deposition process

https://doi.org/10.5194/acp-2021-121
Preprint. Discussion started: 12 March 2021


Atmospheric Chemistry and Physics Discussions

largely counteracting vertical transport. This will leave the chemistry process the major driver of the ozone changes.

We separately sum the quantities of the physical processes and PO_3 contributing to MDA8 surface ozone changes binned to box L. The physical processes lead to -4.83 ppbv changes in the MDA8 ozone mainly due to a relatively larger dry deposition in 2020, whereas $P(O_3)$ contributes to +5.89 ppbv. The net effect is +1.01 ppbv which is slightly smaller than the simulated changes in MDA8 ozone in this region (+1.79 ppbv). This apparent discrepancy is caused by the differences in boundary and initial conditions which are not quantifiable by the process analysis and would require additional sensitivity test. Nonetheless, we believe these numbers should provide convincing evidence on the fact that chemistry has promoted the enhancements of surface ozone during the lockdown.

Chemistry is also a function of meteorology, specifically solar radiation and temperature. A typical scenario to isolate emissions from meteorology is by running the model with fixed anthropogenic emissions (and boundary conditions) and subtracting the outputs from the variable emission output. Figure 11 shows the contribution of anthropogenic emissions (VOCs and NO_x) to the changes seen over the surface. The anthropogenic emissions make up roughly 58% of the changes. The map is strongly in line with the changes in NO_x emissions constrained by TROPOMI. The impact of meteorology plus biogenic changes (the former is dominant) highly correlates with anomalies in both surface air temperature and photolysis rate (Figure 6). We observe negligible ozone changes due to emissions over Iberian Peninsula reinforcing the significance of the meteorological impacts [Ordóñez et al., 2020].

3.4.Ozone chemistry

Figure 12 shows the numerically-solved ozone production rates (PO_3) simulated by the constrained model during the MDA8 hours period. We observe positive PO_3 in less polluted areas and eastern Europe where biomass burning activities occurred in 2019, while negative PO_3 in major cities. Negative values in PO_3 are indicative of either loss in O_3 or O_3-NO-NO_2 partitioning. The difference in PO_3 between the two years suggests that the ozone enhancement in box L is caused by a reduction in negative PO_3 in 2020 over major cities compared to 2019. To examine which pathways are contributing to this pattern, we attempt to analytically reproduce the numerically-solved PO_3 (Figure 12) through two different equations: the first equation widely applied in photochemically active environments follows [Kleinman et al., 2002]:

https://doi.org/10.5194/acp-2021-121
Preprint. Discussion started: 12 March 2021


Atmospheric Chemistry and Physics Discussions

$$P(O_3) = k_{HO_2+NO}[HO_2][NO] + \sum k_{RO_{2i}+NO}[RO_{2i}][NO] - k_{OH+NO_2+M}[OH][NO_2][M] - k_{HO_2+O_3}[HO_2][O_3] - k_{OH+O_3}[OH][O_3] - k_{O(^1D)+H_2O}[O(^1D)][H_2O] - L(O_3 + VOCs) \quad (5)$$

This equation yields negative values only if the O_3 loss pathways including NO_2+OH, HO_x+O_3 , O^1D+H_2O and O_3+VOCs dominate over the first two terms. The second equation which is independent of RO_2 and HO_2 concentrations [Thornton et al., 2002], is:

$$P(O_3) = jNO_2[NO_2] - k_{OH+NO_2+M}[O_3][NO] \quad (6)$$

In summer, this equation tends to be positive during early afternoon, almost zero during afternoon (steady-state), and negative in early morning (or night) in which the second term (O_3 titration) is leading. Any abrupt changes in NO_x and VOC, and photolysis can directly affect equation 6 moving PO_3 out of the diel steady-state. The assumption of the steady-state (PO_3 from equation 6 equals to zero) is also not valid if an air parcel is in the vicinity of high-emitting NO_x sources [Thornton et al., 2002].

Figure 13 displays the reactions rates of each individual component involved in equation 5 averaged during the MDA8 hours. HO_2+NO is the dominant chemical source of ozone correlating well with the changes in NO_x and prevailing chemical conditions regimes (NO_x-sensitive vs VOC-sensitive). Souri et al. [2020a] found the reaction of RO_2+NO to be primarily dependent on VOCs. Likewise, we observe a strong degree of correlation between the anomaly of RO_2+NO and that of VOCs (Figure 3). Figure 13 indicates that the chemical pathways of ozone loss are rather constant between the two years; therefore the largely negative PO_3 over urban areas shown previously in Figure 12 is not reproducible using this equation. Figure 14 shows the reactions rates of $J_{NO2}[NO_2]$, $k_{NO+O3}[NO][O_3]$, and the difference during the MDA8 hours. The difference maps replicate the largely negative PO_3 over cities suggesting that we are not in the diel steady-state, and O_3 titration is prevailing due to relatively low photochemistry in the springtime. Table 4 lists the averaged reactions rates involved in equation 5 and 6 along with the numerically-solved PO_3 shown in Figure 12 over box L. These numbers suggest that the major chemical pathways of enhanced ozone are through $J_{NO2}[NO_2]$ and $k_{NO+O3}[NO][O_3]$, implying that O_3-NO-NO_2 partitioning is more consequential than other chemical pathways. This analysis strongly coincides with Lee et al.

https://doi.org/10.5194/acp-2021-121
Preprint. Discussion started: 12 March 2021


Atmospheric Chemistry and Physics Discussions

[2020] and Wyche et al. [2021] who observed roughly constant O_3+NO_2 concentrations over the UK before and during the lockdown 2020.

4. Summary

The slowdown in human activities due to the COVID-19 pandemic had an immediate and sweeping impact on air pollution over Europe [Barré et al. 2020; Siccard et al., 2020]. Satellite monitoring systems with large spatial coverage help shed light on the spatial and temporal extent of those impacts. The relationships between satellite-derived HCHO and NO_2 columns and near-surface emissions have proven difficult to fully establish without using realistic models, capable of providing insights on the convoluted processes involving chemistry, dynamics, transport, and photochemistry and therefore help with deciphering what anomaly maps of satellite concentrations are suggesting [e.g., Goldberg et al., 2020]. To address these challenges, we jointly constrained NO_x and VOC emissions using TROPOMI HCHO and NO_2 columns following a non-linear Gauss Newton method developed in Souri et al. [2020a], in addition to assimilating MODIS AOD observations based on Jung et al. [2019]. The constrained emissions also permitted investigating the simultaneous effects of physical and chemical processes contributing to ozone formation, illuminating the complexities associated with non-linear chemistry,

Several implications of the derived emissions for the months of March, April, and May 2020 (lockdown) relative to those in 2019 (baseline) were investigated. First, as previously reported [Sicard et al., 2020; Barré et al. 2020], we observed a significant reduction in NO_x in March (14-31%) in several major polluted regions including Paris, London, Madrid, and Milan. The reductions were further seen in other cities such as Rome, Brussels, Frankfurt, Warsaw, Belgrade, Kyiv, and Moscow (34-51%) in April. Second, a large spatial and temporal variability associated with the reduction in NO_x was evident, as each country might have different level and timeline of restrictions. For instance, NO_x emissions decreased drastically in April rather than March in some portions of UK, northern Germany, Moscow, and Poland. Third, we showed that anthropogenic VOC emissions over Paris (-9%), Milan (-29%), London (-5%), and Rome (-5%) decreased in March, a picture that was achievable through jointly using NO_2 and HCHO observations. The reduced anthropogenic VOC emissions were a result of two key assumptions: the reduced NO_x emissions in NO_x-rich areas increased HCHO made from VOCs (evident in larger Jacobians derived from the regional model), and TROPOMI HCHO suggested a negligible difference in HCHO concentration between the two years. This striking result emphasizes the

https://doi.org/10.5194/acp-2021-121
Preprint. Discussion started: 12 March 2021


Atmospheric Chemistry and Physics Discussions

importance of building a multi-specie framework into inverse modeling studies, as the intertwined chemical feedback between HCHO and NO_2 is quite important and shown in proof of concept by Marais et al. [2012], Valin et al. [2016], Wolfe et al. [2016], and Souri et al. [2020b]. Fourth, changes in VOC emissions were primarily dictated by biogenic and biomass burning sources in April and May.

The constrained model calculations gave good representations of near-surface NO_2 changes in April (model: -21±17%, observation: -29±21%) in places where the top-down estimates are reasonable (averaging kernels > 0.5), but inferior representations in other months, especially in May (model: -12±18%, observation: -25±20%). This tendency mainly arose from TROPOMI frequencies; too few days (10-26%) in May due to cloudiness precluded the determination of realistic NO_x emission changes.

We observed surface MDA8 ozone increase from both model and measurements in April 2020 with respect to the baseline. Comparisons of calculation by the constrained model in terms of MDA8 surface ozone found reasonable agreement with observations in the proximity of central Europe in April (model: +3.73±3.94%, +1.79 ppbv, observation: +7.35±11.27%, +3.76 ppbv). These comparisons indicate that the performance of the constrained model to reproduce the ozone enhancement feature is promising, suggesting fruitful information in TROPOMI NO_2 and HCHO, although reasons behind the underestimation of the enhancement remained unexplained. It was clear that the dominantly negative ozone production rates dictated by O_3-NO-NO_2 partitioning ($J_{NO2}[NO_2]$-$k_{NO+O3}[NO][O_3]$) became less negative primarily due to the reduced NO_x emissions in urban areas where O_3 titration occurred. This tendency was in agreement with studies of Lee et al. [2020] and Wyche et al. [2021]. We found negligible differences in ozone production from $[HO_2+RO_2][NO]$ and ozone loss from O^1D+H_2O and O_3+HO_x between the two years suggesting photochemistry was rather low in the springtime over Europe.

We further quantified the contributions of physical processes (transport, diffusion and dry deposition) and chemistry to the formation/loss of ozone using the integrated process rates. The physical processes decreased MDA8 ozone by -4.83 ppbv resulting from relatively larger dry deposition in 2020, whereas chemistry (ozone production) augmented ozone levels by +5.89 ppbv, indicating that rising ozone was primarily impacted by changes in chemistry. Enhanced air temperature and photolysis in 2020, both of which were well captured in our model, also affected chemistry. Experiments with fixed anthropogenic emissions underwent significant enhancement

https://doi.org/10.5194/acp-2021-121
Preprint. Discussion started: 12 March 2021


Atmospheric Chemistry and Physics Discussions

607 in surface MDA8 ozone over central Europe, but those only contribute to 42% of the total
608 enhancement indicating that anthropogenic emissions were the major factor.
609 The results shown here reveal previously unquantified characteristics of ozone and its
610 precursors emission changes during the lockdown 2020 in Europe. We have been able to measure
611 the amount of changes along with the level of confidence in NO_x and VOC emissions using a state-
612 of-the-art inversion technique by leveraging well-characterized satellite observations, which in
613 turn, allowed us to unravel the chemical and physical processes contributing to increased ozone in
614 Europe. Unless a comprehensive air quality campaign targeting COVID-19 related lockdown is
615 available, we recommend that the impact of lockdown on air pollution should be examined through
616 the lens of well-established models constrained by publicly available data, especially those from
617 space in less cloudy environments.
618 **Author contributions**
619 AHS designed the research, analyzed the data, conducted the inverse modeling and atmospheric
620 modeling (for CMAQ, GEOS-Chem, WRF, and MEGAN), made all figures, and wrote the paper.
621 JB validated WRF-CMAQ model and reformatted the surface observation files. CRN and GGA
622 did literature review regarding the TROPOMI validation. YJ validated MODIS AOD. DW helped
623 with implementing the AOD assimilation framework. KC, JM, and XL guided the discussion. All
624 authors contributed to discussion and edited the paper.
625 **Data availability**
626 The atmospheric inversion data are publicly available from Souri et al. [2021]. The model outputs
627 are available upon the request from ahsouri@cfa.harvard.edu. The links on where to download
628 surface and satellite observations that are used in this study are already provided in the text.
629 **Acknowledgments**
630 Amir H. Souri acknowledges supports from the Smithsonian Astrophysical Observatory (SAO)
631 Scholarly Award (40488100AA50203), MethaneSAT LLC, and Environmental Defense Fund. J.
632 Bak acknowledges Basic Science Research Program through the National Research Foundation of
633 Korea (NRF) funded by the Ministry of Education (2020R1A6A1A03044834). Both calculations
634 and simulations are done on the Smithsonian Institution High-Performance Cluster (SI/HPC)
635 (https://doi.org/10.25572/SIHPC). The views expressed in this manuscript are those of the authors
636 alone and do not necessarily reflect the views and policies of the U.S. Environmental Protection
637 Agency. EPA does not endorse any products or commercial services mentioned in this publication.

https://doi.org/10.5194/acp-2021-121
Preprint. Discussion started: 12 March 2021

Atmospheric Chemistry and Physics Discussions

638
639

640 **References**

641 Barré, J., Petetin, H., Colette, A., Guevara, M., Peuch, V.-H., Rouil, L., Engelen, R., Inness, A.,
642 Flemming, J., Pérez García-Pando, C., Bowdalo, D., Meleux, F., Geels, C., Christensen,
643 J. H., Gauss, M., Benedictow, A., Tsyro, S., Friese, E., Struzewska, J., Kaminski, J. W.,
644 Douros, J., Timmermans, R., Robertson, L., Adani, M., Jorba, O., Joly, M. and
645 Kouznetsov, R.: Estimating lockdown induced European NO_2 changes, Atmospheric
646 Chemistry and Physics Discussions, 1–28, https://doi.org/10.5194/acp-2020-995, 2020.
647 Baudic, A., Gros, V., Sauvage, S., Locoge, N., Sanchez, O., Sarda-Estève, R., Kalogridis, C.,
648 Petit, J.-E., Bonnaire, N., Baisnée, D., Favez, O., Albinet, A., Sciare, J. and Bonsang, B.:
649 Seasonal variability and source apportionment of volatile organic compounds (VOCs) in
650 the Paris megacity (France), Atmospheric Chemistry and Physics, 16(18), 11961–11989,
651 https://doi.org/10.5194/acp-16-11961-2016, 2016.
652 Boersma, K. F., Eskes, H. J., Richter, A., De Smedt, I., Lorente, A., Beirle, S., van Geffen, J. H.
653 G. M., Zara, M., Peters, E., Van Roozendael, M., Wagner, T., Maasakkers, J. D., van der
654 A, R. J., Nightingale, J., De Rudder, A., Irie, H., Pinardi, G., Lambert, J.-C. and
655 Compernolle, S. C.: Improving algorithms and uncertainty estimates for satellite NO_2
656 retrievals: results from the quality assurance for the essential climate variables
657 (QA4ECV) project, Atmospheric Measurement Techniques, 11(12), 6651–6678,
658 https://doi.org/10.5194/amt-11-6651-2018, 2018.
659 Castellanos, P. and Boersma, K. F.: Reductions in nitrogen oxides over Europe driven by
660 environmental policy and economic recession, Scientific Reports, 2(1), 265,
661 https://doi.org/10.1038/srep00265, 2012.
662 Chan Miller, C., Jacob, D. J., Marais, E. A., Yu, K., Travis, K. R., Kim, P. S., Fisher, J. A., Zhu,
663 L., Wolfe, G. M., Hanisco, T. F., Keutsch, F. N., Kaiser, J., Min, K.-E., Brown, S. S.,
664 Washenfelder, R. A., González Abad, G. and Chance, K.: Glyoxal yield from isoprene
665 oxidation and relation to formaldehyde: chemical mechanism, constraints from SENEX
666 aircraft observations, and interpretation of OMI satellite data, Atmospheric Chemistry
667 and Physics, 17(14), 8725–8738, https://doi.org/10.5194/acp-17-8725-2017, 2017.
668 Chan, K. L., Wiegner, M., van Geffen, J., De Smedt, I., Alberti, C., Cheng, Z., Ye, S. and Wenig,
669 M.: MAX-DOAS measurements of tropospheric NO2 and HCHO in Munich and the
670 comparison to OMI and TROPOMI satellite observations, Atmospheric Measurement
671 Techniques, 13(8), 4499–4520, https://doi.org/10.5194/amt-13-4499-2020, 2020.
672 Copernicus Sentinel data processed by ESA, German Aerospace Center (DLR) (2019), Sentinel-
673 5P TROPOMI Tropospheric Formaldehyde HCHO 1-Orbit L2 5.5km x 3.5km,
674 Greenbelt, MD, USA, Goddard Earth Sciences Data and Information Services Center
675 (GES DISC), Accessed: [Data Access Date], 10.5270/S5P-tjlxfd2
676 Copernicus Sentinel data processed by ESA, Koninklijk Nederlands Meteorologisch Instituut
677 (KNMI) (2019), Sentinel-5P TROPOMI Tropospheric NO2 1-Orbit L2 5.5km x 3.5km,
678 Greenbelt, MD, USA, Goddard Earth Sciences Data and Information Services Center
679 (GES DISC), Accessed: [Data Access Date], 10.5270/S5P-s4ljg54
680 Coronavirus Disease 2019 (COVID-19) - Daily Situation Report of the Robert Koch Institute".
681 Robert Koch Institute. n.d. Retrieved 30 November 2020.

https://doi.org/10.5194/acp-2021-121
Preprint. Discussion started: 12 March 2021

Atmospheric Chemistry and Physics Discussions

682 Cuchiara, G. C., Li, X., Carvalho, J. and Rappenglück, B.: Intercomparison of planetary
683 boundary layer parameterization and its impacts on surface ozone concentration in the
684 WRF/Chem model for a case study in Houston/Texas, Atmospheric Environment, 96,
685 175–185, https://doi.org/10.1016/j.atmosenv.2014.07.013, 2014.
686 De Smedt, I., Theys, N., Yu, H., Danckaert, T., Lerot, C., Compernolle, S., Van Roozendael, M.,
687 Richter, A., Hilboll, A., Peters, E., Pedergnana, M., Loyola, D., Beirle, S., Wagner, T.,
688 Eskes, H., van Geffen, J., Boersma, K. F. and Veefkind, P.: Algorithm theoretical
689 baseline for formaldehyde retrievals from S5P TROPOMI and from the QA4ECV
690 project, Atmospheric Measurement Techniques, 11(4), 2395–2426,
691 https://doi.org/10.5194/amt-11-2395-2018, 2018.
692 Dickerson, R. R., Anderson, D. C. and Ren, X.: On the use of data from commercial NOx
693 analyzers for air pollution studies, Atmospheric Environment, 214, 116873,
694 https://doi.org/10.1016/j.atmosenv.2019.116873, 2019.
695 Emanuel, K. A.: Atmospheric Convection, 1st edition., Oxford University Press, New York.,
696 1994.
697 Fauci, A. S., Lane, H. C. and Redfield, R. R.: Covid-19 — Navigating the Uncharted, New
698 England Journal of Medicine, 382(13), 1268–1269,
699 https://doi.org/10.1056/NEJMe2002387, 2020.
700 Goldberg, D. L., Anenberg, S. C., Griffin, D., McLinden, C. A., Lu, Z. and Streets, D. G.:
701 Disentangling the Impact of the COVID-19 Lockdowns on Urban NO2 From Natural
702 Variability, Geophysical Research Letters, 47(17), e2020GL089269,
703 https://doi.org/10.1029/2020GL089269, 2020.
704 Grange, S. K., Farren, N. J., Vaughan, A. R., Rose, R. A. and Carslaw, D. C.: Strong
705 Temperature Dependence for Light-Duty Diesel Vehicle NOx Emissions, Environ. Sci.
706 Technol., 53(11), 6587–6596, https://doi.org/10.1021/acs.est.9b01024, 2019.
707 Grell, G. A. and Dévényi, D.: A generalized approach to parameterizing convection combining
708 ensemble and data assimilation techniques, Geophysical Research Letters, 29(14), 38-1-
709 38–4, https://doi.org/10.1029/2002GL015311, 2002.
710 Griffin, D., Zhao, X., McLinden, C. A., Boersma, F., Bourassa, A., Dammers, E., Degenstein,
711 D., Eskes, H., Fehr, L., Fioletov, V., Hayden, K., Kharol, S. K., Li, S.-M., Makar, P.,
712 Martin, R. V., Mihele, C., Mittermeier, R. L., Krotkov, N., Sneep, M., Lamsal, L. N.,
713 Linden, M. ter, Geffen, J. van, Veefkind, P. and Wolde, M.: High-Resolution Mapping of
714 Nitrogen Dioxide With TROPOMI: First Results and Validation Over the Canadian Oil
715 Sands, Geophysical Research Letters, 46(2), 1049–1060,
716 https://doi.org/10.1029/2018GL081095, 2019.
717 Guenther, A. B., Jiang, X., Heald, C. L., Sakulyanontvittaya, T., Duhl, T., Emmons, L. K. and
718 Wang, X.: The Model of Emissions of Gases and Aerosols from Nature version 2.1
719 (MEGAN2.1): an extended and updated framework for modeling biogenic emissions,
720 Geoscientific Model Development, 5(6), 1471–1492, https://doi.org/10.5194/gmd-5-
721 1471-2012, 2012.
722 He, G., Pan, Y. and Tanaka, T.: The short-term impacts of COVID-19 lockdown on urban air
723 pollution in China, Nature Sustainability, 3(12), 1005–1011,
724 https://doi.org/10.1038/s41893-020-0581-y, 2020.
725 Hoesly, R. M., Smith, S. J., Feng, L., Klimont, Z., Janssens-Maenhout, G., Pitkanen, T., Seibert,
726 J. J., Vu, L., Andres, R. J., Bolt, R. M., Bond, T. C., Dawidowski, L., Kholod, N.,
727 Kurokawa, J., Li, M., Liu, L., Lu, Z., Moura, M. C. P., O'Rourke, P. R. and Zhang, Q.:

Historical (1750–2014) anthropogenic emissions of reactive gases and aerosols from the Community Emissions Data System (CEDS), Geoscientific Model Development, 11(1), 369–408, https://doi.org/10.5194/gmd-11-369-2018, 2018.

Jacob, D. J.: Heterogeneous chemistry and tropospheric ozone, Atmospheric Environment, 34(12), 2131–2159, https://doi.org/10.1016/S1352-2310(99)00462-8, 2000.

Jacobson, M. Z.: Fundamentals of Atmospheric Modeling, 2nd ed., Cambridge University Press, Cambridge., 2005.

Janjić, T., Bormann, N., Bocquet, M., Carton, J. A., Cohn, S. E., Dance, S. L., Losa, S. N., Nichols, N. K., Potthast, R., Waller, J. A. and Weston, P.: On the representation error in data assimilation, Quarterly Journal of the Royal Meteorological Society, 144(713), 1257–1278, https://doi.org/10.1002/qj.3130, 2018.

Judd, L. M., Al-Saadi, J. A., Szykman, J. J., Valin, L. C., Janz, S. J., Kowalewski, M. G., Eskes, H. J., Veefkind, J. P., Cede, A., Mueller, M., Gebetsberger, M., Swap, R., Pierce, R. B., Nowlan, C. R., Abad, G. G., Nehrir, A. and Williams, D.: Evaluating Sentinel-5P TROPOMI tropospheric NO2 column densities with airborne and Pandora spectrometers near New York City and Long Island Sound, Atmospheric Measurement Techniques, 13(11), 6113–6140, https://doi.org/10.5194/amt-13-6113-2020, 2020.

Jung, J., Souri, A. H., Wong, D. C., Lee, S., Jeon, W., Kim, J. and Choi, Y.: The Impact of the Direct Effect of Aerosols on Meteorology and Air Quality Using Aerosol Optical Depth Assimilation During the KORUS-AQ Campaign, Journal of Geophysical Research: Atmospheres, 124(14), 8303–8319, https://doi.org/10.1029/2019JD030641, 2019.

Karlsson, P. E., Ferm, M., Tømmervik, H., Hole, L. R., Pihl Karlsson, G., Ruoho-Airola, T., Aas, W., Hellsten, S., Akselsson, C., Mikkelsen, T. N. and Nihlgård, B.: Biomass burning in eastern Europe during spring 2006 caused high deposition of ammonium in northern Fennoscandia, Environmental Pollution, 176, 71–79, https://doi.org/10.1016/j.envpol.2012.12.006, 2013.

Ke, Y., Leung, L. R., Huang, M., Coleman, A. M., Li, H. and Wigmosta, M. S.: Development of high resolution land surface parameters for the Community Land Model, Geoscientific Model Development, 5(6), 1341–1362, https://doi.org/10.5194/gmd-5-1341-2012, 2012.

Krotkov, N. A., McLinden, C. A., Li, C., Lamsal, L. N., Celarier, E. A., Marchenko, S. V., Swartz, W. H., Bucsela, E. J., Joiner, J., Duncan, B. N., Boersma, K. F., Veefkind, J. P., Levelt, P. F., Fioletov, V. E., Dickerson, R. R., He, H., Lu, Z. and Streets, D. G.: Aura OMI observations of regional SO_2 and NO_2 pollution changes from 2005 to 2015, Atmospheric Chemistry and Physics, 16(7), 4605–4629, https://doi.org/10.5194/acp-16-4605-2016, 2016.

Kleinman, L. I., Daum, P. H., Lee, Y.-N., Nunnermacker, L. J., Springston, S. R., Weinstein-Lloyd, J. and Rudolph, J.: Ozone production efficiency in an urban area, Journal of Geophysical Research: Atmospheres, 107(D23), ACH 23-1-ACH 23-12, https://doi.org/10.1029/2002JD002529, 2002.

Lambert, J.-C., Compernole, S., Eichmann, K.-U., Graaf, M. de, Hubert, D., Keppens, A., Kleipool, Q., Langerock, B., Sha, M. K., Verhoelst, T., Wagner, T., Ahn, C., Argyrouli, A., Balis, D., Chan, K. L., Smedt, I. De, Eskes, H., Fjæraa, A. M., Garane, K., Gleason, J. F., Goutail, F., Granville, J., Hedelt, P., Heue, K.-P., Jaross, G., Koukouli, M., Landgraf, J., Lutz, R., Nanda, S., Niemejer, S., Pazmiño, A., Pinardi, G., Pommereau, J.-P., Richter, A., Rozemeijer, N., Sneep, M., Zweers, D. S., Theys, N., Tilstra, G., Torres, O., Valks, P., Vigouroux, C., Wang, P. and Weber, M.: Quarterly Validation Report of the

https://doi.org/10.5194/acp-2021-121
Preprint. Discussion started: 12 March 2021

Atmospheric Chemistry and Physics Discussions

774 Copernicus Sentinel-5 Precursor Operational Data Products #06: April 2018 - February
775 2020. [online]
776 Lamsal, L. N., Martin, R. V., Donkelaar, A. van, Steinbacher, M., Celarier, E. A., Bucsela, E.,
777 Dunlea, E. J. and Pinto, J. P.: Ground-level nitrogen dioxide concentrations inferred from
778 the satellite-borne Ozone Monitoring Instrument, Journal of Geophysical Research:
779 Atmospheres, 113(D16), https://doi.org/10.1029/2007JD009235, 2008.
780 Le Quéré, C., Jackson, R. B., Jones, M. W., Smith, A. J. P., Abernethy, S., Andrew, R. M., De-
781 Gol, A. J., Willis, D. R., Shan, Y., Canadell, J. G., Friedlingstein, P., Creutzig, F. and
782 Peters, G. P.: Temporary reduction in daily global CO 2 emissions during the COVID-19
783 forced confinement, Nature Climate Change, 10(7), 647–653,
784 https://doi.org/10.1038/s41558-020-0797-x, 2020.
785 Le, T., Wang, Y., Liu, L., Yang, J., Yung, Y. L., Li, G. and Seinfeld, J. H.: Unexpected air
786 pollution with marked emission reductions during the COVID-19 outbreak in China,
787 Science, 369(6504), 702–706, https://doi.org/10.1126/science.abb7431, 2020.
788 Lee, J. D., Drysdale, W. S., Finch, D. P., Wilde, S. E. and Palmer, P. I.: UK surface NO_2 levels
789 dropped by 42 % during the COVID-19 lockdown: impact on surface O_3,
790 Atmospheric Chemistry and Physics, 20(24), 15743–15759, https://doi.org/10.5194/acp-
791 20-15743-2020, 2020.
792 Levy, R. C., Mattoo, S., Munchak, L. A., Remer, L. A., Sayer, A. M., Patadia, F. and Hsu, N. C.:
793 The Collection 6 MODIS aerosol products over land and ocean, Atmospheric
794 Measurement Techniques, 6(11), 2989–3034, https://doi.org/10.5194/amt-6-2989-2013,
795 2013.
796 Li, K. and Lin, B.: Impacts of urbanization and industrialization on energy consumption/CO2
797 emissions: Does the level of development matter?, Renewable and Sustainable Energy
798 Reviews, 52, 1107–1122, https://doi.org/10.1016/j.rser.2015.07.185, 2015.
799 Li, K., Jacob, D. J., Liao, H., Shen, L., Zhang, Q. and Bates, K. H.: Anthropogenic drivers of
800 2013–2017 trends in summer surface ozone in China, PNAS, 116(2), 422–427,
801 https://doi.org/10.1073/pnas.1812168116, 2019.
802 Lin, Y.-L., Farley, R. D. and Orville, H. D.: Bulk Parameterization of the Snow Field in a Cloud
803 Model, Journal of Applied Meteorology and Climatology, 22(6), 1065–1092,
804 https://doi.org/10.1175/1520-0450(1983)022<1065:BPOTSF>2.0.CO;2, 1983.
805 Liu, F., Page, A., Strode, S. A., Yoshida, Y., Choi, S., Zheng, B., Lamsal, L. N., Li, C., Krotkov,
806 N. A., Eskes, H., A, R. van der, Veefkind, P., Levelt, P. F., Hauser, O. P. and Joiner, J.:
807 Abrupt decline in tropospheric nitrogen dioxide over China after the outbreak of COVID-
808 19, Science Advances, 6(28), eabc2992, https://doi.org/10.1126/sciadv.abc2992, 2020.
809 Lorenz, E. N.: Deterministic Nonperiodic Flow, Journal of the Atmospheric Sciences, 20(2),
810 130–141, https://doi.org/10.1175/1520-0469(1963)020<0130:DNF>2.0.CO;2, 1963.
811 Madronich, S.: Photodissociation in the atmosphere: 1. Actinic flux and the effects of ground
812 reflections and clouds, Journal of Geophysical Research: Atmospheres, 92(D8), 9740–
813 9752, https://doi.org/10.1029/JD092iD08p09740, 1987.
814 Marais, E. A., Jacob, D. J., Kurosu, T. P., Chance, K., Murphy, J. G., Reeves, C., Mills, G.,
815 Casadio, S., Millet, D. B., Barkley, M. P., Paulot, F. and Mao, J.: Isoprene emissions in
816 Africa inferred from OMI observations of formaldehyde columns, Atmospheric
817 Chemistry and Physics, 12(14), 6219–6235, https://doi.org/10.5194/acp-12-6219-2012,
818 2012.

https://doi.org/10.5194/acp-2021-121
Preprint. Discussion started: 12 March 2021

819 Miyazaki, K., Bowman, K., Sekiya, T., Jiang, Z., Chen, X., Eskes, H., Ru, M., Zhang, Y. and
820 Shindell, D.: Air Quality Response in China Linked to the 2019 Novel Coronavirus
821 (COVID-19) Lockdown, Geophysical Research Letters, 47(19), e2020GL089252,
822 https://doi.org/10.1029/2020GL089252, 2020.
823 Nevius, D. S. and Evans, C.: The Influence of Vertical Advection Discretization in the WRF-
824 ARW Model on Capping Inversion Representation in Warm-Season, Thunderstorm-
825 Supporting Environments, Weather and Forecasting, 33(6), 1639–1660,
826 https://doi.org/10.1175/WAF-D-18-0103.1, 2018.
827 Ordóñez, C., Garrido-Perez, J. M. and García-Herrera, R.: Early spring near-surface ozone in
828 Europe during the COVID-19 shutdown: Meteorological effects outweigh emission
829 changes, Science of The Total Environment, 747, 141322,
830 https://doi.org/10.1016/j.scitotenv.2020.141322, 2020.
831 Parrish, D. D., Lamarque, J.-F., Naik, V., Horowitz, L., Shindell, D. T., Staehelin, J., Derwent,
832 R., Cooper, O. R., Tanimoto, H., Volz-Thomas, A., Gilge, S., Scheel, H.-E., Steinbacher,
833 M. and Fröhlich, M.: Long-term changes in lower tropospheric baseline ozone
834 concentrations: Comparing chemistry-climate models and observations at northern
835 midlatitudes, Journal of Geophysical Research: Atmospheres, 119(9), 5719–5736,
836 https://doi.org/10.1002/2013JD021435, 2014.
837 Pleim, J. E.: A Combined Local and Nonlocal Closure Model for the Atmospheric Boundary
838 Layer. Part I: Model Description and Testing, Journal of Applied Meteorology and
839 Climatology, 46(9), 1383–1395, https://doi.org/10.1175/JAM2539.1, 2007.
840 Possanzini, M., Palo, V. D. and Cecinato, A.: Sources and photodecomposition of formaldehyde
841 and acetaldehyde in Rome ambient air, Atmospheric Environment, 36(19), 3195–3201,
842 https://doi.org/10.1016/S1352-2310(02)00192-9, 2002.
843 Pusede, S. E., Steiner, A. L. and Cohen, R. C.: Temperature and Recent Trends in the Chemistry
844 of Continental Surface Ozone, Chem. Rev., 115(10), 3898–3918,
845 https://doi.org/10.1021/cr5006815, 2015.
846 Salma, I., Vörösmarty, M., Gyöngyösi, A. Z., Thén, W. and Weidinger, T.: What can we learn
847 about urban air quality with regard to the first outbreak of the COVID-19 pandemic? A
848 case study from central Europe, Atmospheric Chemistry and Physics, 20(24), 15725–
849 15742, https://doi.org/10.5194/acp-20-15725-2020, 2020.
850 Schneidemesser, E. von, Monks, P. S., Gros, V., Gauduin, J. and Sanchez, O.: How important is
851 biogenic isoprene in an urban environment? A study in London and Paris, Geophysical
852 Research Letters, 38(19), https://doi.org/10.1029/2011GL048647, 2011.
853 Seinfeld, J. H. and Pandis, S. N.: Atmospheric Chemistry and Physics: From Air Pollution to
854 Climate Change, 2nd edition., Wiley-Interscience, Hoboken, N.J., 2006.
855 Shi, X. and Brasseur, G. P.: The Response in Air Quality to the Reduction of Chinese Economic
856 Activities During the COVID-19 Outbreak, Geophysical Research Letters, 47(11),
857 e2020GL088070, https://doi.org/10.1029/2020GL088070, 2020.
858 Sicard, P., De Marco, A., Agathokleous, E., Feng, Z., Xu, X., Paoletti, E., Rodriguez, J. J. D. and
859 Calatayud, V.: Amplified ozone pollution in cities during the COVID-19 lockdown,
860 Science of The Total Environment, 735, 139542,
861 https://doi.org/10.1016/j.scitotenv.2020.139542, 2020.
862 Sillman, S.: The relation between ozone, NOx and hydrocarbons in urban and polluted rural
863 environments, Atmospheric Environment, 33(12), 1821–1845,
864 https://doi.org/10.1016/S1352-2310(98)00345-8, 1999.

https://doi.org/10.5194/acp-2021-121
Preprint. Discussion started: 12 March 2021

865 Silvern, R. F., Jacob, D. J., Mickley, L. J., Sulprizio, M. P., Travis, K. R., Marais, E. A., Cohen,
866 R. C., Laughner, J. L., Choi, S., Joiner, J. and Lamsal, L. N.: Using satellite observations
867 of tropospheric NO_2 columns to infer long-term trends in US NO_x emissions: the
868 importance of accounting for the free tropospheric NO_2 background, Atmospheric
869 Chemistry and Physics, 19(13), 8863–8878, https://doi.org/10.5194/acp-19-8863-2019,
870 2019.
871 Skamarock, W. C. and Klemp, J. B.: A time-split nonhydrostatic atmospheric model for weather
872 research and forecasting applications, Journal of Computational Physics, 227(7), 3465–
873 3485, https://doi.org/10.1016/j.jcp.2007.01.037, 2008.
874 Souri, A. H., Nowlan, C. R., González Abad, G., Zhu, L., Blake, D. R., Fried, A., Weinheimer,
875 A. J., Wisthaler, A., Woo, J.-H., Zhang, Q., Chan Miller, C. E., Liu, X. and Chance, K.:
876 An inversion of NO_x and non-methane volatile organic compound (NMVOC) emissions
877 using satellite observations during the KORUS-AQ campaign and implications for
878 surface ozone over East Asia, Atmospheric Chemistry and Physics, 20(16), 9837–9854,
879 https://doi.org/10.5194/acp-20-9837-2020, 2020a.
880 Souri, A. H., Nowlan, C. R., Wolfe, G. M., Lamsal, L. N., Chan Miller, C. E., Abad, G. G., Janz,
881 S. J., Fried, A., Blake, D. R., Weinheimer, A. J., Diskin, G. S., Liu, X. and Chance, K.:
882 Revisiting the effectiveness of HCHO/NO2 ratios for inferring ozone sensitivity to its
883 precursors using high resolution airborne remote sensing observations in a high ozone
884 episode during the KORUS-AQ campaign, Atmospheric Environment, 224, 117341,
885 https://doi.org/10.1016/j.atmosenv.2020.117341, 2020b.
886 Souri, Amir H., Chance, K., Bak, J., Nowlan, C., González Abad, G., Jung, Y., Wong, D., Mao,
887 J., Liu, X.: COVID-19-Europe-Ozone-NOx-VOC, Mendeley Data, V1, doi:
888 10.17632/jchfxsrvsb.1, 2021
889 Stavrakou, T., Müller, J.-F., Bauwens, M., De Smedt, I., Van Roozendael, M., Guenther, A.,
890 Wild, M. and Xia, X.: Isoprene emissions over Asia 1979–2012: impact of climate
891 and land-use changes, Atmospheric Chemistry and Physics, 14(9), 4587–4605,
892 https://doi.org/10.5194/acp-14-4587-2014, 2014.
893 Su, T., Li, Z. and Kahn, R.: Relationships between the planetary boundary layer height and
894 surface pollutants derived from lidar observations over China: regional pattern and
895 influencing factors, Atmospheric Chemistry and Physics, 18(21), 15921–15935,
896 https://doi.org/10.5194/acp-18-15921-2018, 2018.
897 Thornton, J. A., Wooldridge, P. J., Cohen, R. C., Martinez, M., Harder, H., Brune, W. H.,
898 Williams, E. J., Roberts, J. M., Fehsenfeld, F. C., Hall, S. R., Shetter, R. E., Wert, B. P.
899 and Fried, A.: Ozone production rates as a function of NOx abundances and HOx
900 production rates in the Nashville urban plume, Journal of Geophysical Research:
901 Atmospheres, 107(D12), ACH 7-1-ACH 7-17, https://doi.org/10.1029/2001JD000932,
902 2002.
903 United Nations Conference on Trade and Development Report, Accessed Dec 2020,
904 https://unctad.org/system/files/official-document/dtltlbinf2020d1_en.pdf
905 Valin, L. C., Fiore, A. M., Chance, K. and Abad, G. G.: The role of OH production in
906 interpreting the variability of CH2O columns in the southeast U.S., Journal of
907 Geophysical Research: Atmospheres, 121(1), 478–493,
908 https://doi.org/10.1002/2015JD024012, 2016.
909 Verhoelst, T., Compernolle, S., Pinardi, G., Lambert, J.-C., Eskes, H. J., Eichmann, K.-U.,
910 Fjæraa, A. M., Granville, J., Niemeijer, S., Cede, A., Tiefengraber, M., Hendrick, F.,

https://doi.org/10.5194/acp-2021-121
Preprint. Discussion started: 12 March 2021

Atmospheric Chemistry and Physics Discussions

Pazmiño, A., Bais, A., Bazureau, A., Boersma, K. F., Bognar, K., Dehn, A., Donner, S., Elokhov, A., Gebetsberger, M., Goutail, F., Grutter de la Mora, M., Gruzdev, A., Gratsea, M., Hansen, G. H., Irie, H., Jepsen, N., Kanaya, Y., Karagkiozidis, D., Kivi, R., Kreher, K., Levelt, P. F., Liu, C., Müller, M., Navarro Comas, M., Piters, A. J. M., Pommereau, J.-P., Portafaix, T., Prados-Roman, C., Puentedura, O., Querel, R., Remmers, J., Richter, A., Rimmer, J., Rivera Cárdenas, C., Saavedra de Miguel, L., Sinyakov, V. P., Stremme, W., Strong, K., Van Roozendael, M., Veefkind, J. P., Wagner, T., Wittrock, F., Yela González, M. and Zehner, C.: Ground-based validation of the Copernicus Sentinel-5P TROPOMI NO2 measurements with the NDACC ZSL-DOAS, MAX-DOAS and Pandonia global networks, Atmospheric Measurement Techniques, 14(1), 481–510, https://doi.org/10.5194/amt-14-481-2021, 2021.

Vigouroux, C., Langerock, B., Bauer Aquino, C. A., Blumenstock, T., Cheng, Z., De Mazière, M., De Smedt, I., Grutter, M., Hannigan, J. W., Jones, N., Kivi, R., Loyola, D., Lutsch, E., Mahieu, E., Makarova, M., Metzger, J.-M., Morino, I., Murata, I., Nagahama, T., Notholt, J., Ortega, I., Palm, M., Pinardi, G., Röhling, A., Smale, D., Stremme, W., Strong, K., Sussmann, R., Té, Y., van Roozendael, M., Wang, P. and Winkler, H.: TROPOMI–Sentinel-5 Precursor formaldehyde validation using an extensive network of ground-based Fourier-transform infrared stations, Atmospheric Measurement Techniques, 13(7), 3751–3767, https://doi.org/10.5194/amt-13-3751-2020, 2020.

Wyche, K. P., Nichols, M., Parfitt, H., Beckett, P., Gregg, D. J., Smallbone, K. L. and Monks, P. S.: Changes in ambient air quality and atmospheric composition and reactivity in the South East of the UK as a result of the COVID-19 lockdown, Science of The Total Environment, 755, 142526, https://doi.org/10.1016/j.scitotenv.2020.142526, 2021.

Wang, P., Piters, A., van Geffen, J., Tuinder, O., Stammes, P. and Kinne, S.: Shipborne MAX-DOAS measurements for validation of TROPOMI NO_2 products, Atmospheric Measurement Techniques, 13(3), 1413–1426, https://doi.org/10.5194/amt-13-1413-2020, 2020.

Wang, W., Parrish, D. D., Li, X., Shao, M., Liu, Y., Mo, Z., Lu, S., Hu, M., Fang, X., Wu, Y., Zeng, L. and Zhang, Y.: Exploring the drivers of the increased ozone production in Beijing in summertime during 2005–2016, Atmospheric Chemistry and Physics, 20(24), 15617–15633, https://doi.org/10.5194/acp-20-15617-2020, 2020.

Wolfe, G. M., Kaiser, J., Hanisco, T. F., Keutsch, F. N., de Gouw, J. A., Gilman, J. B., Graus, M., Hatch, C. D., Holloway, J., Horowitz, L. W., Lee, B. H., Lerner, B. M., Lopez-Hilifiker, F., Mao, J., Marvin, M. R., Peischl, J., Pollack, I. B., Roberts, J. M., Ryerson, T. B., Thornton, J. A., Veres, P. R. and Warneke, C.: Formaldehyde production from isoprene oxidation across NO_x regimes, Atmospheric Chemistry and Physics, 16(4), 2597–2610, https://doi.org/10.5194/acp-16-2597-2016, 2016.

Xiu, A. and Pleim, J. E.: Development of a Land Surface Model. Part I: Application in a Mesoscale Meteorological Model, Journal of Applied Meteorology and Climatology, 40(2), 192–209, https://doi.org/10.1175/1520-0450(2001)040<0192:DOALSM>2.0.CO;2, 2001.

Zhao, X., Griffin, D., Fioletov, V., McLinden, C., Cede, A., Tiefengraber, M., Müller, M., Bognar, K., Strong, K., Boersma, F., Eskes, H., Davies, J., Ogyu, A. and Lee, S. C.: Assessment of the quality of TROPOMI high-spatial-resolution NO_2 data products in the Greater Toronto Area, Atmospheric Measurement Techniques, 13(4), 2131–2159, https://doi.org/10.5194/amt-13-2131-2020, 2020.

https://doi.org/10.5194/acp-2021-121
Preprint. Discussion started: 12 March 2021

Atmospheric Chemistry and Physics Discussions

957
958
959
960
961
962 **Table 1.** Statistics reported in several validations studies comparing TROPOMI
963 tropospheric NO_2 against independent observations.
964

Study	Location	Time Period	Benchmark Instrument	Bias (low)	RMSE	Modification	Modified Bias (low)
Chan et al. 2020	Munich	May 2018-Apr 2019	MAXDOAS	30%	N/A	In-situ MAX-DOAS profiles	17%
Griffin et al. 2019	Canadian Oil Sands	Mar-May 2018 (v1.01)	Pandora (direct Sun)	15-30%	N/A	Higher resolution profiles (10 km) and albedo	0-25%
Judd et al. 2020	New York	Jun-Sep 2018	GeoTASO	19-33%	N/A	Higher resolution profiles (12 km)	7-19%
Verhoelst et al. 2020	Global	Apr 2018-Feb 2020	MAXDOAS	37% (average), 23-51% (range)	3.5×10^{15} molec/cm^2	N/A	N/A
Wang P. et al. 2020	Atlantic and Pacific Oceans	4 campaigns during Dec 2018-Jul 2019	MAXDOAS	Negligible	N/A	N/A	N/A
Zhao et al. 2020	Greater Toronto Area	Mar 2018-Mar 2019	Pandora (direct Sun)	24-28% (suburban/urban) +4-10% (rural)		Higher resolution profiles (10 km) and albedo	13-24% (suburban/urban) +14-15% (rural)

965
966
967
968
969

https://doi.org/10.5194/acp-2021-121
Preprint. Discussion started: 12 March 2021

Atmospheric Chemistry and Physics Discussions

Table 2. Relative and absolute differences of top-down estimate of NO_x emissions using TROPOMI for different countries in Europe in March-May 2020 (lockdown) with respect to 2019 (baseline). Ton and d denote tonne and day, respectively.

Countries	March (%, ton/d)		April (%, ton/d)		May (%, ton/d)	
Austria	-17.25	-63.36	-6.64	-23.32	-3.77	-12.17
Belarus	-12.99	-67.91	-15.39	-88.86	-4.22	-19.85
Belgium	-32.6	-159.34	-27.31	-137.95	-28.61	-177.56
Czech Republic	-23.66	-113.31	-9.74	-43.50	-2.85	-11.31
Denmark	-10.88	-17.91	-13.12	-29.58	-8.12	-19.84
Finland	-2.88	-5.92	-7.70	-18.21	-8.82	-19.39
France	-25.35	-547.20	-20.46	-467.45	-9.29	-198.17
Germany	-7.2	-203.63	-24.42	-832.93	-9.58	-285.57
Greece	-20.56	-77.88	-5.32	-19.91	-0.88	-3.38
Hungary	-12.24	-34.31	-6.21	-18.57	-5.01	-12.25
Ireland	-12.5	-24.55	-7.48	-16.83	-3.73	-8.15
Italy	-17.81	-270.57	-16.14	-252.17	+2.37	34.15
Netherlands	+8.86	28.30	-9.71	-38.99	-2.27	-10.98
Norway	-2.88	-7.69	-8.87	-26.91	-3.40	-9.52
Poland	-15.05	-246.15	-20.02	-342.90	-8.34	-126.70
Portugal	-8.83	-24.42	-8.80	-23.31	-3.39	-10.16
Romania	-12.93	-70.83	-1.13	-5.80	+1.12	5.25
Spain	-10.13	-156.21	-12.53	-192.19	-2.12	-32.45
Sweden	-6.60	-15.17	-8.94	-23.12	-6.48	-15.85
Switzerland	-8.46	-14.15	-8.03	-13.23	-13.07	-18.96
Turkey	-10.46	-224.27	-3.97	-76.61	-5.22	-98.66
Ukraine	-13.64	-224.24	-12.31	-198.00	-13.82	-207.06
United Kingdom	-14.94	-254.82	-19.11	-334.27	-14.35	-263.89
The strait of Gibraltar and Alboran Sea	-7.17	-77.32	-8.58	-86.69	-14.34	-10.67
All	**-13.93 ± 8.44**	**-2795.65 ± 129.67**	**-15.4 ± 6.70**	**-3224.62 ± 194.51**	**-7.72 ± 6.52**	**-1522.46 ± 92.00**

https://doi.org/10.5194/acp-2021-121
Preprint. Discussion started: 12 March 2021

Atmospheric Chemistry and Physics Discussions

Table 3. Relative and absolute differences of top-down estimate of VOC emissions using TROPOMI for different cities in Europe in March 2020 (lockdown) and 2019 (baseline).

Countries	March 2020 (ton/d)	March 2019 (ton/d)	Diff (%, ton/d)	
Paris	54.27	59.66	-9.03	-5.39
Rome	9.92	10.46	-5.18	-0.54
Milan	1.83	2.59	-29.40	-0.76
London	27.74	29.32	-5.38	-1.58

Table 4. Reaction rates relating to the chemical pathways of ozone formation and loss over box L (proximity of central Europe).

Reactions	Production (P) or loss (L)	April 2020 (ppbv/hr)	April 2019 (ppbv/hr)	Net diff [a](ppbv/hr)
HO_2+NO	P	0.85	0.91	-0.06
RO_2+NO	P	0.44	0.41	+0.03
NO_2+OH	L	0.10	0.14	+0.04
O^1D+H_2O	L	0.07	0.08	+0.01
O_3+VOCs	L	0.01	0.01	0.00
O_3+HO_x	L	0.09	0.08	-0.01
$J_{NO2}[NO_2]$	P	14.61	27.28	-12.67
$k_{NO+O3}[NO][O_3]$	L	15.11	28.52	+13.40
$J_{NO2}[NO_2]$- $k_{NO+O3}[NO][O_3]$	N/A	-0.50	-1.24	+0.74
Numerically solved PO_3	N/A	-0.79	-1.53	+0.74

[a] A positive net difference indicates higher (lower) production (loss) in 2020 with respect to 2019.

https://doi.org/10.5194/acp-2021-121
Preprint. Discussion started: 12 March 2021

Atmospheric Chemistry and Physics Discussions

984

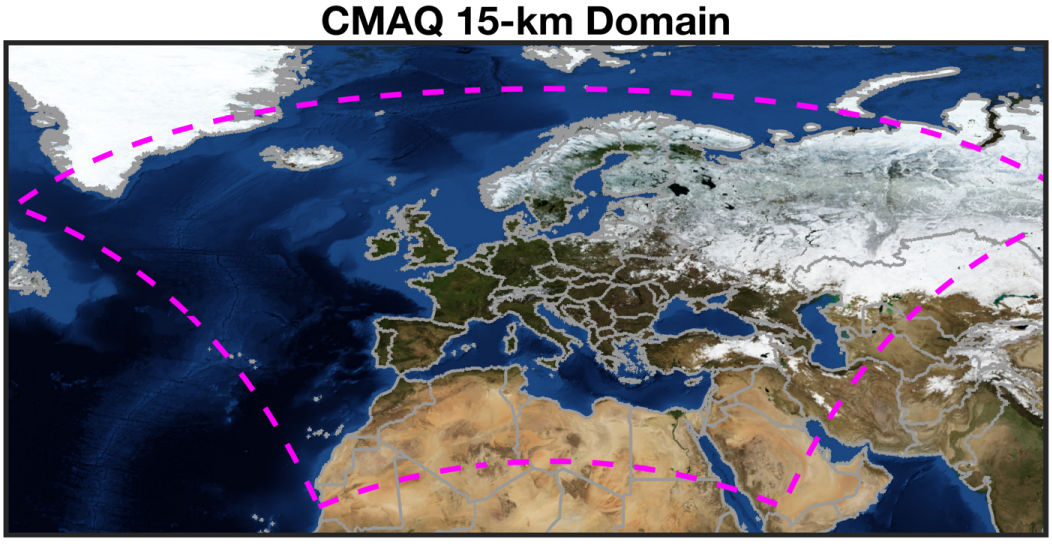

985

986 **Figure 1.** The WRF-CMAQ 15 km domain covering Europe. The background picture is based
987 on the publicly available NASA Blue Marble (© NASA).
988

https://doi.org/10.5194/acp-2021-121
Preprint. Discussion started: 12 March 2021

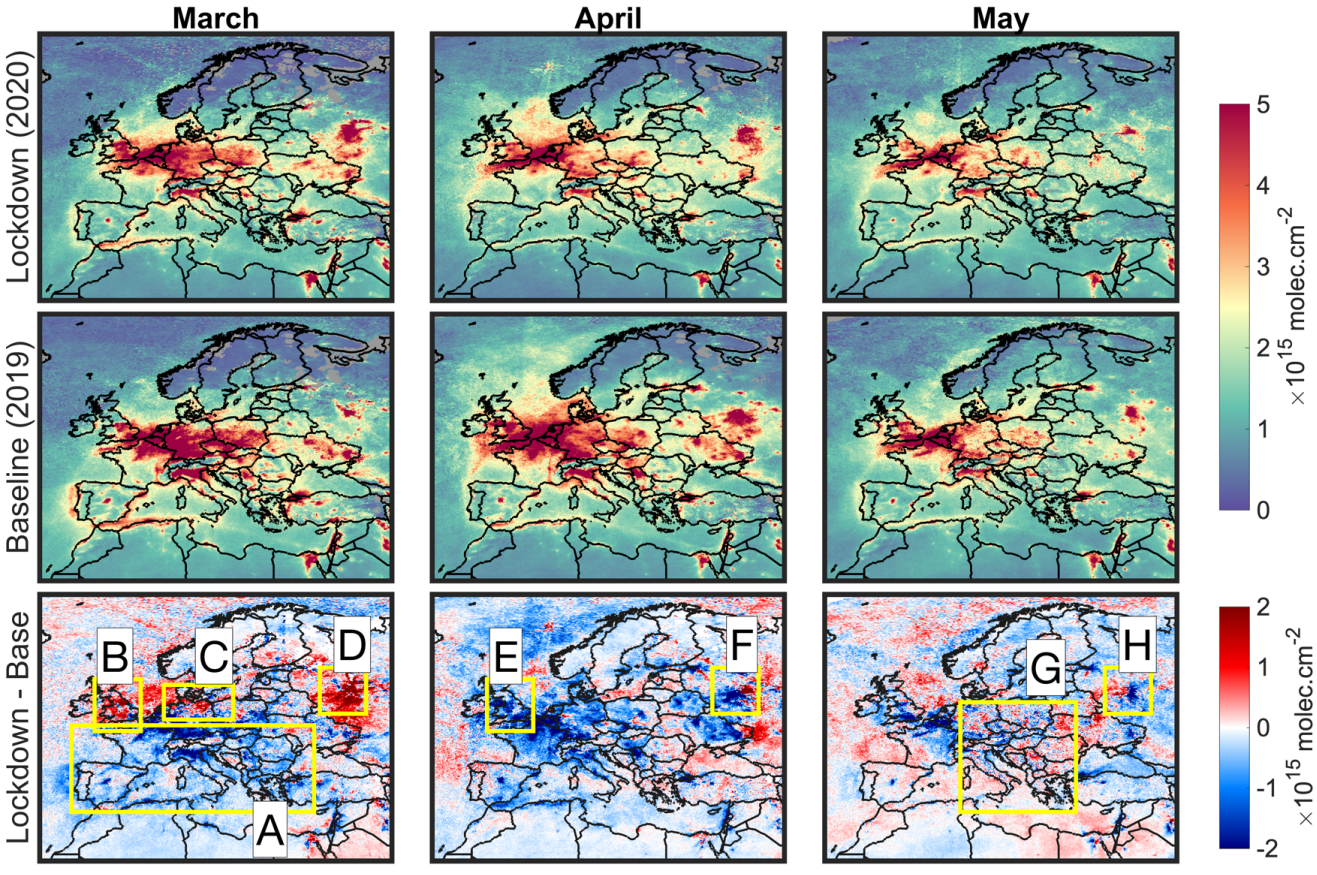

Figure 2. (first row) Contour maps of tropospheric NO_2 from the TROPOMI sensor during months of March, April, and May in 2020 (lockdown). (second row) Same as the first row but for the baseline year (2019). (last row), Difference of the columns in 2020 with respect to those of 2019. All columns are corrected for the bias and their AMFs are recalculated iteratively based on the posterior profiles derived from our inverse modeling practice. The satellite-derived columns are subject to errors, so a direct interpretation of their magnitudes cannot be performed in a robust manner.

https://doi.org/10.5194/acp-2021-121
Preprint. Discussion started: 12 March 2021

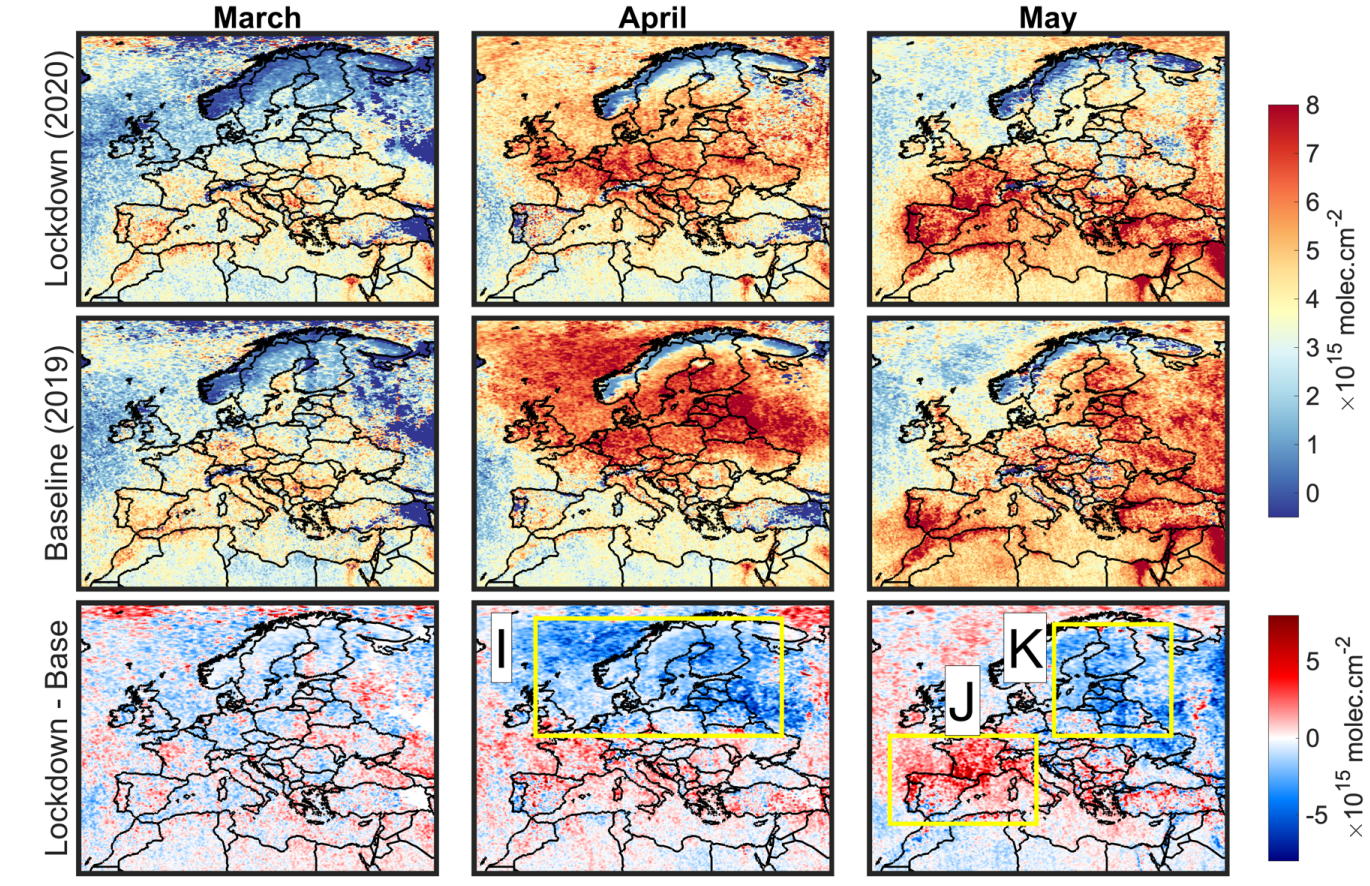

1001 **Figure 3.** Same as Figure 2 but for the total HCHO columns.

1002

1003

https://doi.org/10.5194/acp-2021-121
Preprint. Discussion started: 12 March 2021

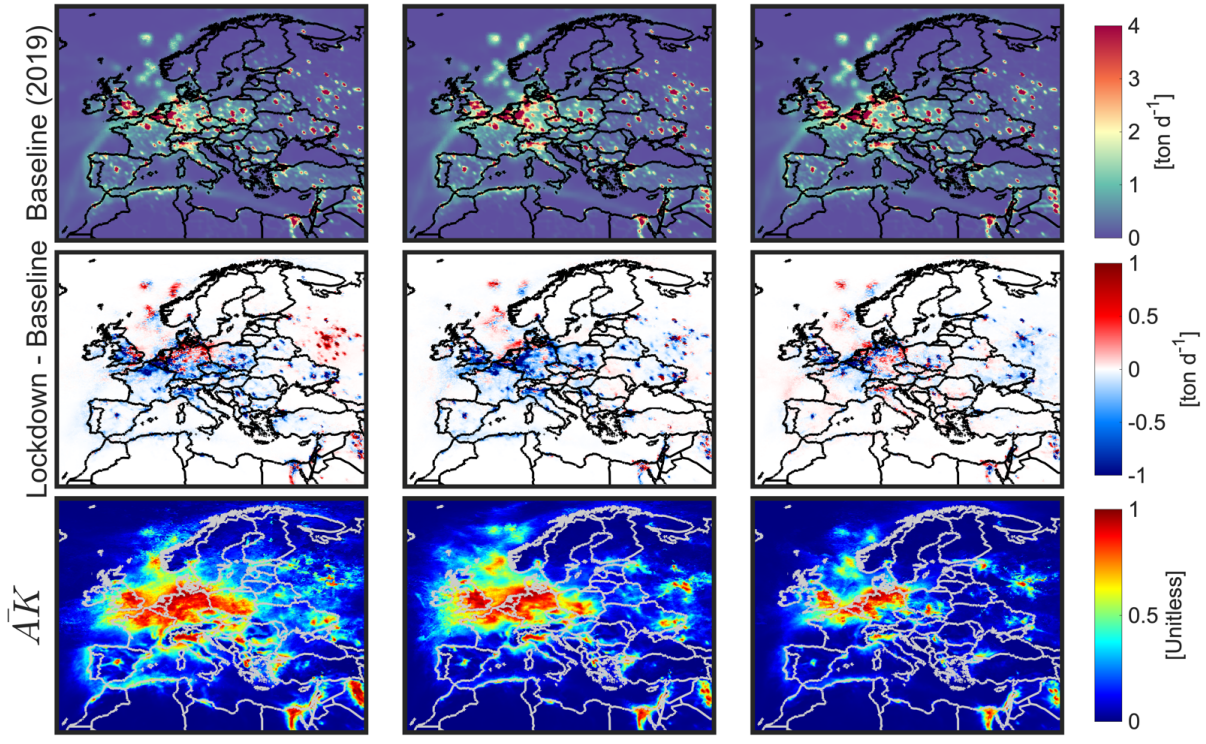

Figure 4. Top-down estimates of total NO_x during months of March, April and May in 2019 (baseline) and the differences with respect to 2020. To infer the magnitude of emissions in 2020, the second row should be added to the first one. Both TROPOMI HCHO and NO_2 observations are jointly used to estimate these numbers. Averaging kernels (mean values based on both 2019 and 2020 estimates) explain the level of credibility of the estimate which is heavily dependent on the TROPOMI signal/noise ratios.

https://doi.org/10.5194/acp-2021-121
Preprint. Discussion started: 12 March 2021

Atmospheric Chemistry and Physics Discussions

1012

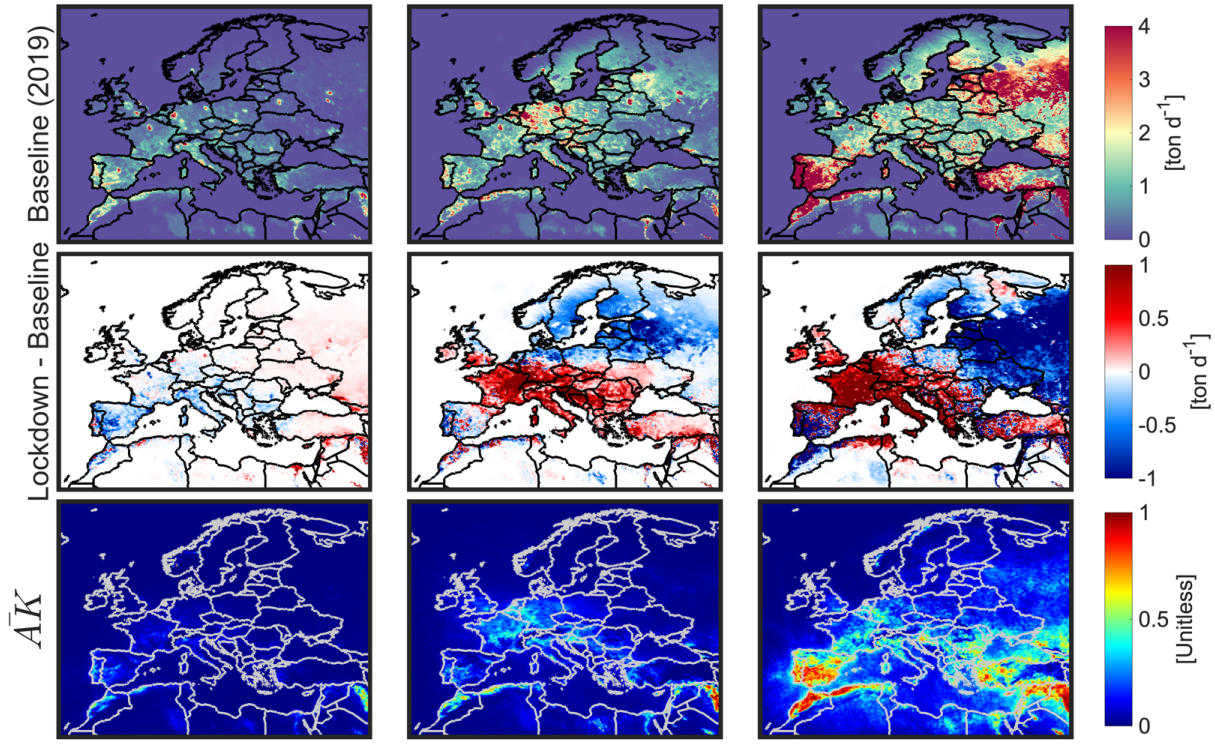

101

1014 **Figure 5.** Same as Figure 4 but for the total VOC emissions.

1015

1016

1017

https://doi.org/10.5194/acp-2021-121
Preprint. Discussion started: 12 March 2021

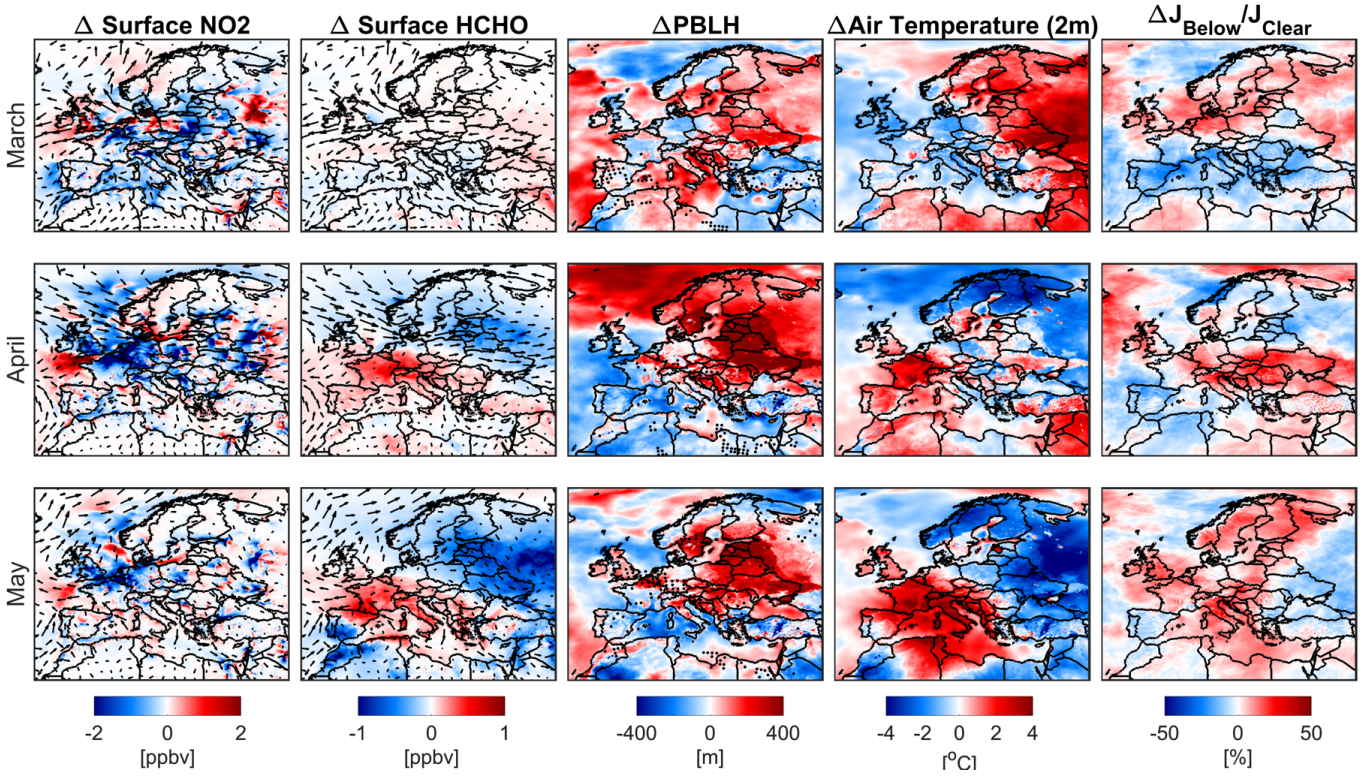

1019 **Figure 6.** Daily-averaged differences in simulated surface NO_2, HCHO, surface wind vectors,
1020 PBLH, surface air temperature, and the ratio of photolysis rate below clouds to a clear-sky
1021 condition. The difference maps are computed by subtracting values in 2020 from those in 2019.
1022 Black dots overlaid in the PBLH subplot denote calm surface winds (<1 m/s).
1023

https://doi.org/10.5194/acp-2021-121
Preprint. Discussion started: 12 March 2021

1024

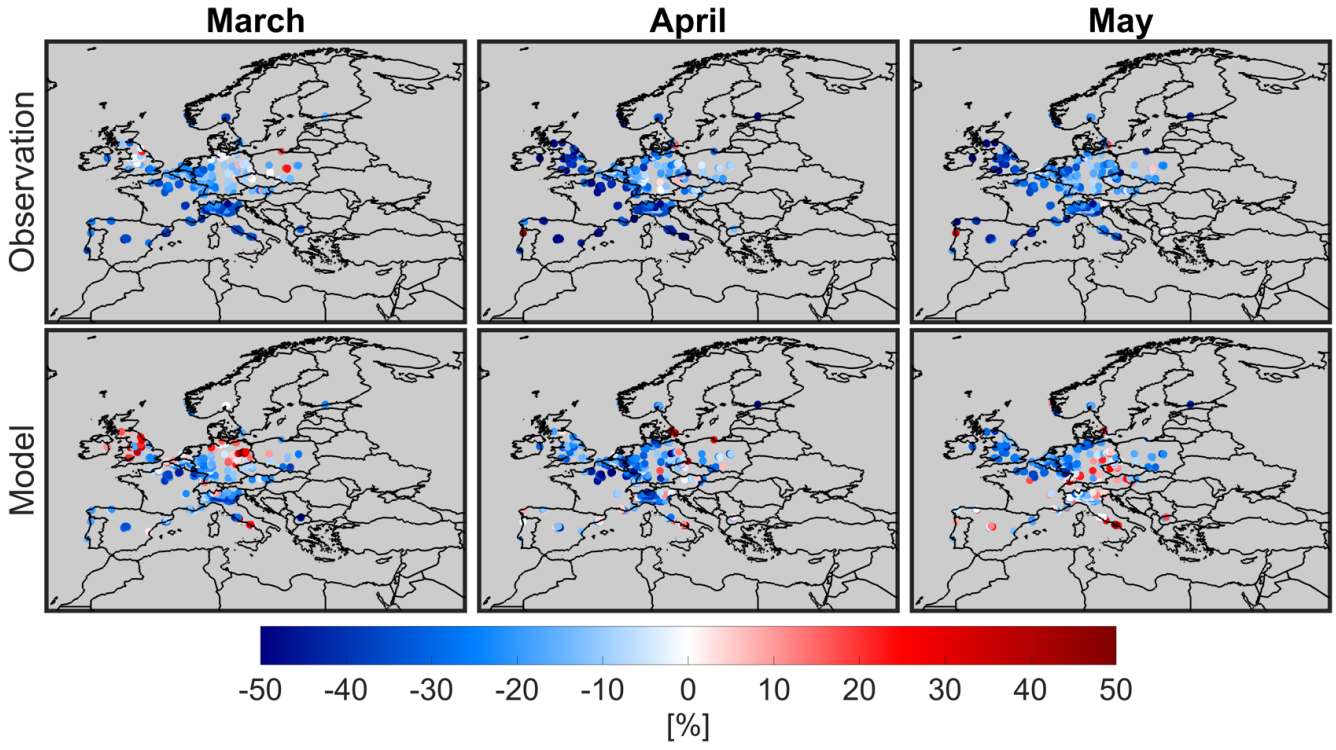

1026 **Figure 7.** Scatter maps of relative changes in surface NO_2 concentrations suggested by the
1027 European air quality network (first row), and the constrained model (second row). Results are
1028 daily-averaged. We only consider grid cells whose averaging kernels (from the NO_x inversion)
1029 are above 0.5. Furthermore, grid cells having more than 2 stations are only included to partly
1030 account for the spatial representivity factor. Surface concentrations are not accounted for the
1031 NO_z family interferences.
1032

https://doi.org/10.5194/acp-2021-121
Preprint. Discussion started: 12 March 2021

1033

1034

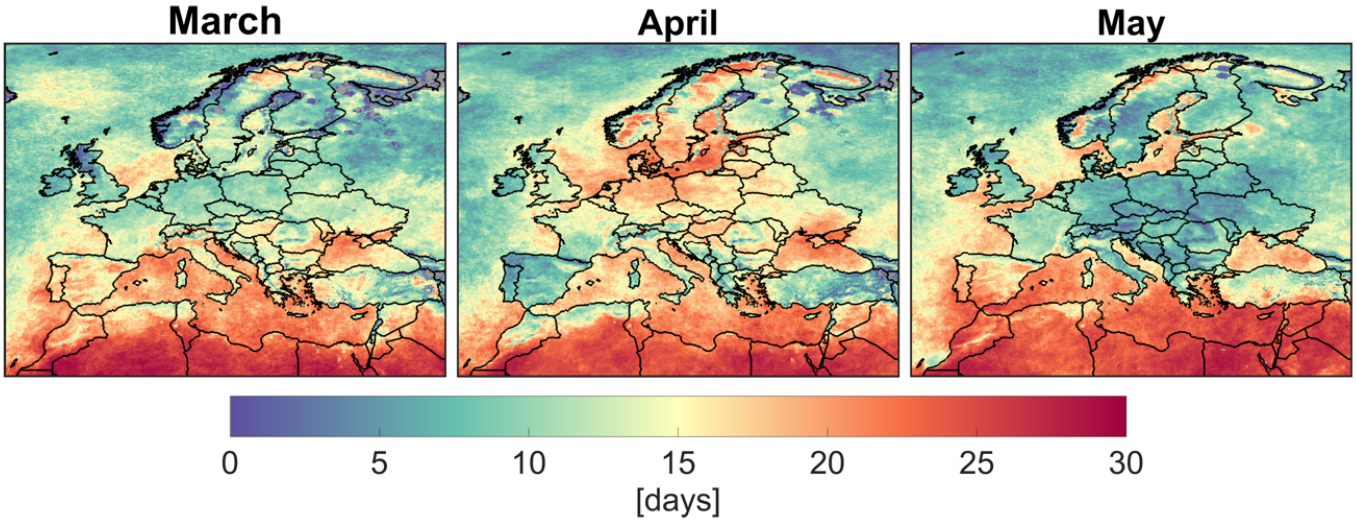

1036 **Figure 8.** Number of good quality (qa_flag>0.75) TROPOMI tropospheric NO_2 days observed at
1037 15×15 km^2. These numbers are heavily affected by cloudiness.

1038

https://doi.org/10.5194/acp-2021-121
Preprint. Discussion started: 12 March 2021

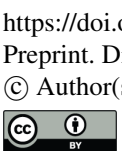

Atmospheric Chemistry and Physics Discussions

1039

1040

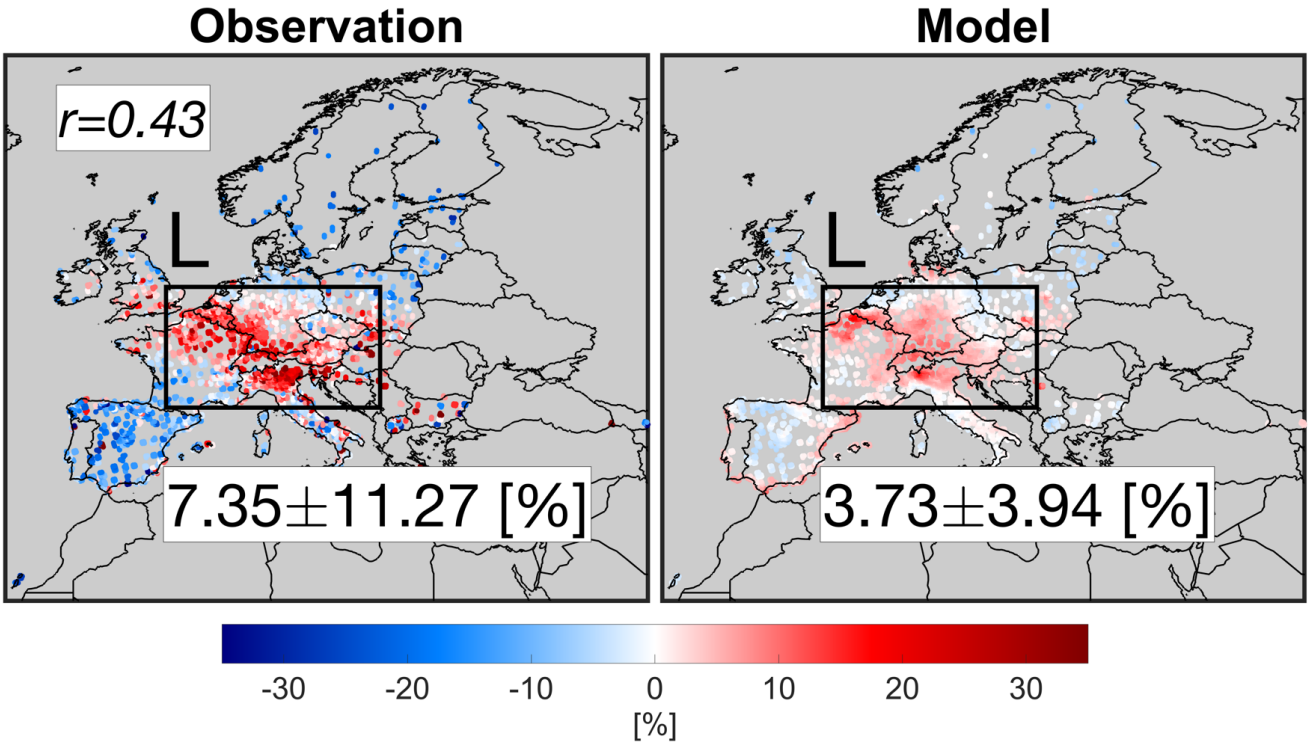

1042 **Figure 9.** Changes in surface MDA8 ozone concentrations suggested by the observation (left),
1043 and the constrained model (right) in April 2020 relative to those in 2019.

1044

https://doi.org/10.5194/acp-2021-121
Preprint. Discussion started: 12 March 2021

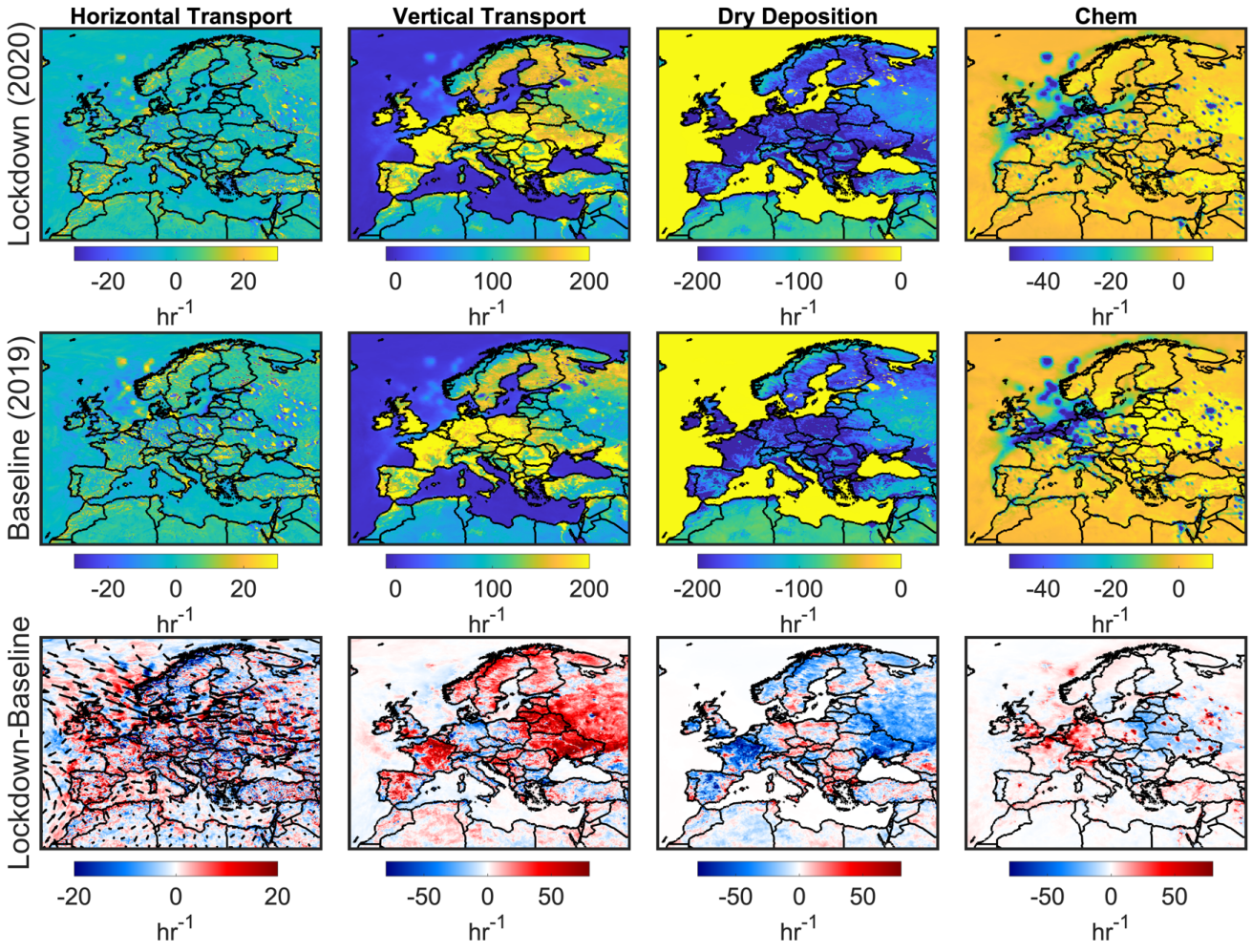

1048 **Figure 10.** Surface process tendencies (hr^{-1}) including horizontal transport (advection plus
1049 diffusion), vertical transport (advection plus diffusion), dry deposition, and chemistry. Positive
1050 (negative) values mean source (sink) of ozone. These outputs are based on the constrained
1051 model. Wind vectors are the difference.

https://doi.org/10.5194/acp-2021-121
Preprint. Discussion started: 12 March 2021

Atmospheric Chemistry and Physics Discussions

1053

1054

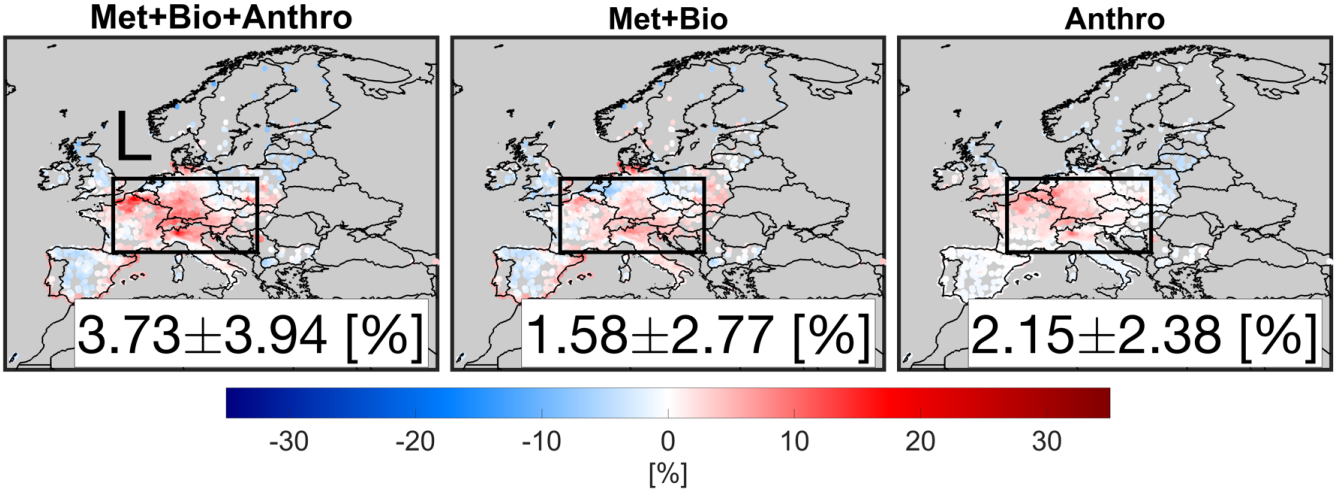

1056 **Figure 11.** Simulated MDA8 surface ozone difference between April 2020 with respect to April
1057 2019 including (left) dynamical meteorology, biogenic and anthropogenic emissions, (middle)
1058 dynamical meteorology and biogenic emissions, and (right) the subtraction of the previous
1059 scenarios isolating dynamical anthropogenic emissions.

1060

1061

https://doi.org/10.5194/acp-2021-121
Preprint. Discussion started: 12 March 2021

Atmospheric Chemistry and Physics Discussions

1062

1063

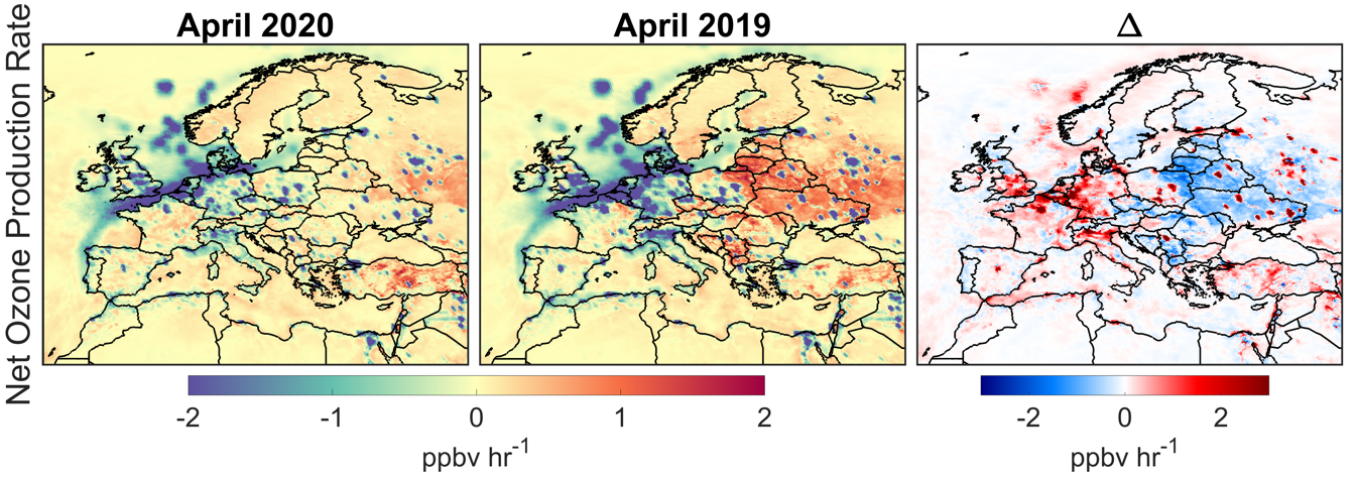

1065 **Figure 12.** Numerically-solved net ozone production rates based on the WRF-CMAQ simulations
1066 using constrained emissions in April 2020, 2019, and the difference. These values are over the
1067 surface and are averaged during the MDA8 hours.

1068

https://doi.org/10.5194/acp-2021-121
Preprint. Discussion started: 12 March 2021

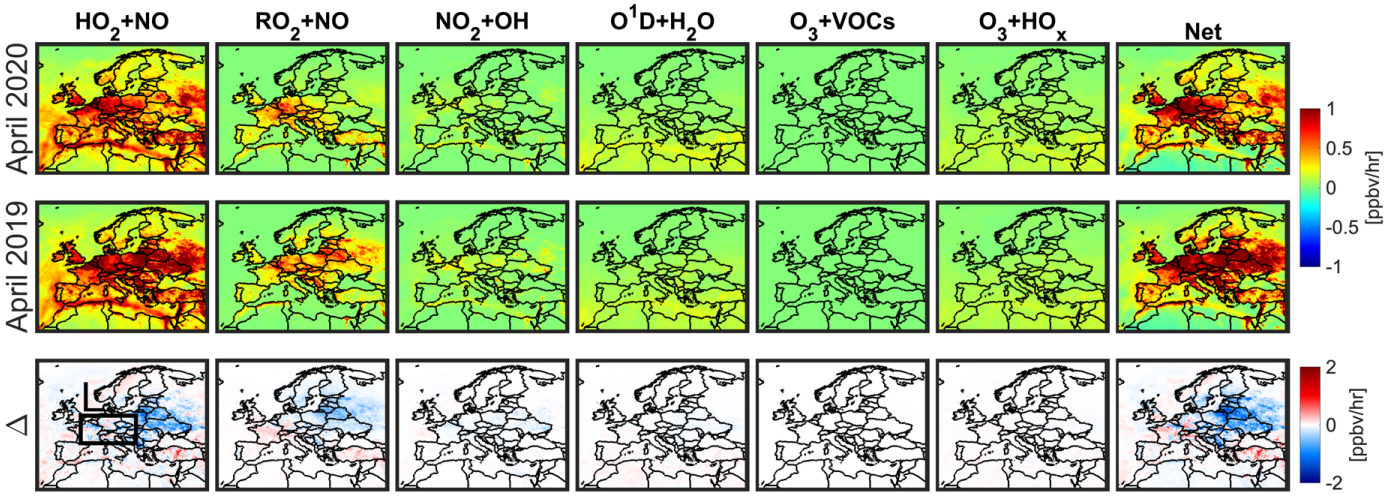

1070 **Figure 13.** Surface chemical processes involved in equation 5 (ppbv hr^{-1}) pertaining to the
1071 production and loss of ozone in April 2020 (lockdown) and 2019 (baseline) during MDA8 hours.
1072

https://doi.org/10.5194/acp-2021-121
Preprint. Discussion started: 12 March 2021

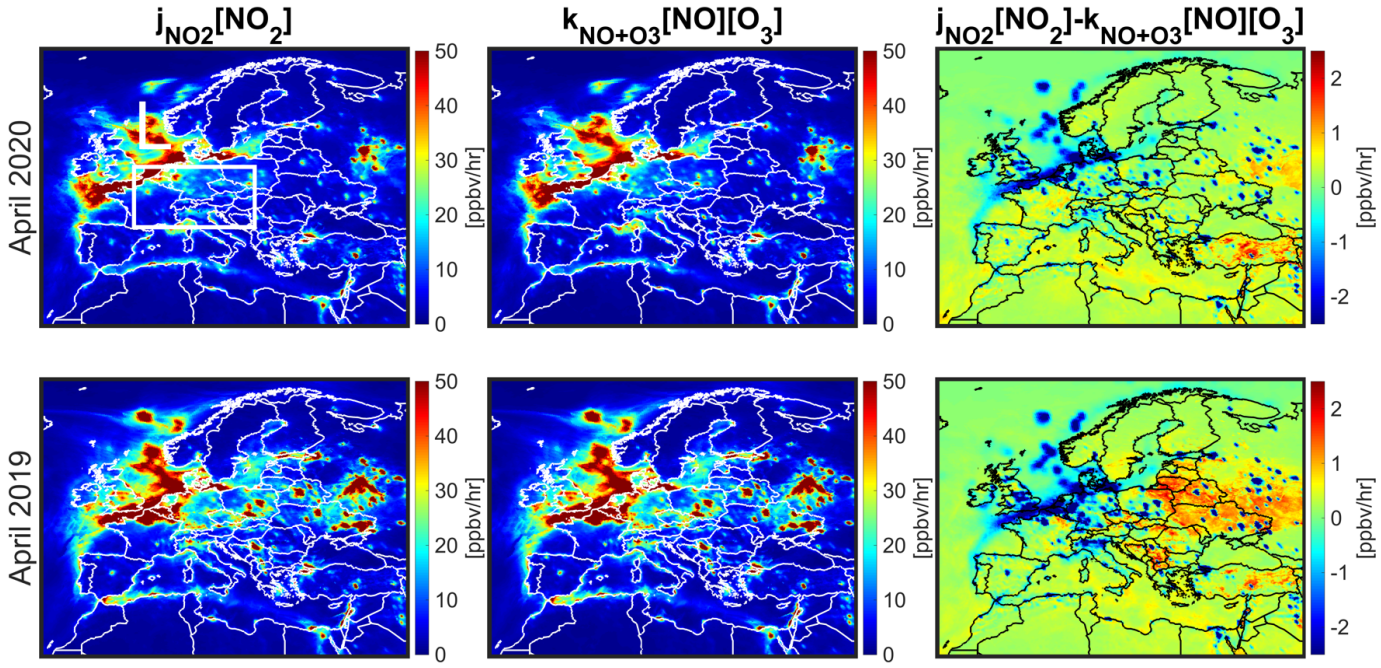

1074 **Figure 14.** Surface chemical processes involved in equation 6 (ppbv hr^{-1}) pertaining to the O_3-
1075 NO-NO_2 partitioning in April 2020 and 2019 during MDA8 hours.
1076
1077
1078